DEGREE OF MIXING DOWNSTREAM OF RECTANGULAR BENDS AND DESIGN OF AN INLET FOR AMBIENT AEROSOL

A Thesis

by

YOUNGJIN SEO

Submitted to the Office of Graduate Studies of
Texas A&M University
in partial fulfillment of the requirements for the degree of

MASTER OF SCIENCE

December 2004

Major Subject: Mechanical Engineering

DEGREE OF MIXING DOWNSTREAM OF RECTANGULAR BENDS

AND DESIGN OF AN INLET FOR AMBIENT AEROSOL

A Thesis

by

YOUNGJIN SEO

Submitted to Texas A&M University
in partial fulfillment of the requirements
for the degree of

MASTER OF SCIENCE

Approved as to style and content by:

Andrew R. McFarland (Co-Chair of Committee)	Dennis L. O'Neal (Co-Chair of Committee)
Yassin A. Hassan (Member)	Dennis L. O'Neal (Head of Department)

December 2004

Major Subject: Mechanical Engineering

ABSTRACT

Degree of Mixing Downstream of Rectangular Bends

and Design of an Inlet for Ambient Aerosol. (December 2004)

Youngjin Seo, B.S., Hankuk Aviation University, Koyang, Korea

Co-Chairs of Advisory Committee: Dr. Andrew R. McFarland
Dr. Dennis L. O'Neal

Tests were conducted to characterize mixing in a square and a rectangular duct with respect to suitability for single point sampling of contaminants. Several configurations, such as a straight duct with unidirectional flow at the entrance section and straight ducts preceded by mixing elements (a 90° mitred bend, double 90° bends in S- and U-type configurations) were tested. For a straight duct of square cross section, the *COV* of tracer gas concentration at 19 duct diameters downstream of the gas release location is 143% (Center release). *COV*s of velocity and tracer gas concentration downstream of each mixing element in square duct setups were verified throughout this study. In the case of a rectangular duct with a 3:1 (width to height) aspect ratio, *COV*s of velocity and tracer gas concentration only downstream of a 90° mitred bend were verified.

Tests were conducted to develop improved inlets for a Battelle bioaerosol sampling system. New inlets have been developed called the All Weather Inlets (AWI), which are designed to prevent entry of precipitation while maintaining aerosol penetration. The AWI has two inlets - one that samples at a flow rate of 780 L/min and the other one that is

operated at a flow rate of 90 L/min. The initial version of the AWI-780 L/min unit featured an internal cone, which was removed because the penetration of the AWI-780 without the bottom chamber was higher than that of the Battelle inlet – 81% with the cone while 86% without the cone for around 9.5 μm AD at 2 km/h. The best bug-screen configuration was verified and a cutpoint management process was performed. The inlets were tested with different wind speeds from 2 to 24 km/h to verify the wind sensitivity of those inlets.

ACKNOWLEDGMENTS

I would like to express my appreciation and gratitude to my advisors, Drs. Andrew R. McFarland and Dennis L. O'Neal, for their encouragement, guidance, and advice. Especially, Dr. McFarland's patience inspired me to work much harder. Without their help, I couldn't have made this achievement happen. I also thank Dr. Yassin A. Hassan for being my committee member and for his advice.

This research was funded by REDCOM, U.S. Army, and their financial support for this work is gratefully acknowledged.

I also want to express many thanks to Mr. Carlos Ortiz for his well experienced ideas, technical assistance, and advice while conducting experiments. I thank Drs. John Haglund and Sridhar Hari for their suggestions and for the helpful discussions. I thank all the ATL personnel for their time and support.

Finally, I would like to express many thanks to my lovely wife, Jiyoung Park for her support during my study here at Texas A&M University.

ABLE OF CONTENTS

CHAPTER Page

Page

LIST OF FIGURES

Page

Page

Page

LIST OF TABLES

Page

CHAPTER I

INTRODUCTION

This thesis consists of four chapters. The first chapter contains the general introduction for Chapter II and III and the last chapter contains the general conclusion. Chapter II, DEGREE OF MIXING DOWNSTREAM OF RECTANGULAR BENDS, mainly deals with characterizing mixing in a square and a rectangular duct preceded by several mixing elements (a 90° mitred bend and double 90° in S- and U-type configurations). Chapter III, DESIGN OF AN INLET FOR AMBIENT AEROSOL, explains about how to design, upgrade, and test an inlet for ambient aerosol.

This thesis follows style and format of *Aerosol Science and Technology*.

CHAPTER II

DEGREE OF MIXING DOWNSTREAM OF RECTANGULAR BENDS*

2.1. PREFACE

2.1.1. Background

There is concern in the U.S. about the possibility of hazardous bioaerosols being released in occupied environments. If such an event were to occur, with current technology, it is likely that detection of a release for alarm purposes could best be accomplished by extractive sampling from air conditioning ducts. The question then arises as to how best to extract the sample in terms of the sampling location and the methodology for accomplishing the sampling. For detection purposes, the bioaerosol aerosol concentration in the duct must not be significantly underestimated, and if dose is to be inferred, the sample should be representative of the mean concentration in the ductwork.

Typically the protocol for extractive sampling of particulate matter has been based on the assumption that retrospective analyses will be used. For example, for regulatory compliance, batch samples of particulate matter are routinely taken from stacks of industrial sources using EPA Methods 5 and 17 technology (U.S. EPA, 2000a and 2000b, respectively), which involve isokinetic extraction of sub-samples from points are specified in EPA Method 1 (EPA 2000c). Assuming there are minimal

---

*Submitted to Health Physics for peer review for publication. If the manuscript is published, copyright will be assigned to Health Physics.

temporal variations in aerosol concentration during the sampling period, this methodology provides accurate estimates on the rate of emission of particulate matter because the combination of traversing and isokinetic extraction is tantamount to a spatial averaging the aerosol concentration. However, the method is not suitable for continuous extractive sampling as is needed for continuous monitoring of bioaerosols.

There are two problems that preclude use of methodology similar to that of EPA Methods 5 and 17 in continuous monitoring applications. First, because the EPA Methods are for batch sampling, internal wall losses of sample can be recovered after a test. For continuous monitoring, these losses are not recoverable in the time period of interest and thus these losses degrade the sampling process. Second, it is not practical to either scan across a duct to obtain a representative sample or to setup rakes of nozzles across the duct cross section to try to achieve assurance that the sample will not underestimate the concentration of contaminant. Any bioaerosol challenge would tend to be highly time dependent, which eliminates consideration of a scanning tactic. The use of rakes of isokinetic nozzles entails deployment of smaller nozzle diameters than would be associated with single point sampling. Small-sized nozzles can cause significant losses of particulate matter. Fan et al. (1993) measured 25% transmission (75% loss) of 10 μm AD particles in a 6 mm diameter isokinetic nozzle of a rake assembly at a gas velocity of 10 m/s, where the nozzles were designed to be in compliance with an early version of an ANSI standard (ANSI, 1969) for sampling of the emissions from stacks and ducts of the nuclear industry. Here, transmission is the ratio of mean aerosol concentration at the exit plane of a probe to the aerosol concentration in the undisturbed flow stream at the probe location. In contrast, Rodgers et al. (1996) used single point sampling with a shrouded

probe (McFarland et al., 1989; Chandra and McFarland, 1997) and observed 98% to 105% transmission of 1-20 μm AD aerosol through the probe at a stack velocity of 24 m/s.

The nuclear industry is confronted with a problem similar to that for bioaerosol sampling from ductwork. Under the requirements of 40 CFR 61, Subparts H and I, the U.S. Environmental Protection Agency (U.S. EPA, 2003d and 2003e) requires new federal nuclear facilities that can potentially emit significant quantities of radionuclides to be continuously monitored using the methodology recommended in American National Standards Institute N13.1 (HPS/ANSI, 1999). The ANSI methodology is based on the concept that a representative sample can best be obtained from a single point in the flow field at a location where both fluid momentum and contaminant mass are relatively uniform as manifested by the shapes of the velocity and contaminant concentration profiles. This approach, which was proposed by McFarland and Rodgers (1993), ensures that the concentration at the point where the sample is extracted will not significantly underestimate the average concentration. Further, by using a single nozzle rather than a rake of nozzles, the penetration of aerosol through the nozzle can be made to be close to 100%.

2.1.2. Single Point Representative Sampling

The ANSI N13.1 criteria for acceptability of a location for single point representative sampling are:

1. The coefficients of variation (*COV*s) of gas velocity, tracer gas and 10 μm aerodynamic diameter (AD) aerosol particles must be ≤ 20% over an area that includes at least the central 2/3 of the duct cross sectional area. The points at

which the measurements are made are typically those of the appropriate EPA Method 1 grid of traverse points

2. The swirl angle of the flow must not exceed 20°, where the swirl is measured using the protocol of EPA Method 1, and the angle is the average of absolute flow angles at all of the traverse points on an EPA Method 1 grid at the sampling location. The swirl at a point is defined as the angle between the duct axis and the fluid velocity vector. Typically, the swirl angle is measured as the yaw angle between flow and duct axes.
3. The maximum value of tracer gas at any point on an EPA Method 1 grid at the sampling location shall not deviate from the mean by more than 30%.

Here, a *COV* of a set of measurements is defined as:

$$COV = \frac{\sqrt{\frac{1}{N-1}\sum_{i=1}^{N}(x_i - \bar{x})^2}}{\bar{x}} \qquad (1)$$

where x_i is the value of either the tracer gas concentration or velocity at i_{th} the sampling point, N is the number of sampling points at a cross-sectional area, and $\bar{x}$ is the mean value of all measured values at a cross-sectional area, and is given by

$$\bar{x} = \frac{1}{N}\sum_{i=1}^{N} x_i \qquad (2)$$

Several studies (Gupta 1999; McFarland et al. 1999b; McFarland et al. 1999a; Anand et al. 2003; Ballinger et al. 2004) have been conducted to characterize mixing in nuclear stacks and the general results can be summarized as: 1) mixing in a duct is driven by the large-scale turbulent eddies, which effectively transfer mass and momentum across the duct; 2) the generators for the large turbulent eddies are flow disturbances (e.g., bends)

upstream of the test section; 3) The mixing process is primarily dependent upon geometry and not on flow properties (e.g., Reynolds number) provided the flow is well into the turbulent flow regime; and, 4) the *COV*s are progressively lower at larger distances in a straight duct downstream of a mixing element (i.e., large eddy turbulence generator).

The previous studies on mixing to achieve suitable conditions for single point representative sampling dealt with ducts of circular geometry. Because much of the ductwork in large commercial or governmental buildings is of rectangular geometry, tests were conducted to characterize mixing in square and rectangular ducts, and to compare the results with those for circular ducts. The goal of this effort is to provide a basis for selection of sampling locations in the rectangular ducts.

2.1.3. Hydraulic Diameter of a Rectangular Duct

Dimensionless distance in the axial direction of the duct is expressed as the ratio of L/D_H where L is the actual length and D_H is the hydraulic diameter. In turn, the hydraulic diameter is expressed as (Fox and McDonald, 2001):

$$D_H = \frac{4A}{P_w} \qquad (3)$$

where: A = cross sectional area of the duct; and, P_w is the perimeter of the duct cross sectional area. For a square duct that has a side width of W, the hydraulic diameter is:

$$D_H = W \qquad (4)$$

For a rectangular duct that has a cross section of $W \times H$, the hydraulic diameter is:

$$D_H = \frac{2(W \times H)}{W + H} \qquad (5)$$

where H is the duct dimension normal to W.

2.2. EXPERIMENTAL PROTOCOL

2.2.1. General

Tests were conducted to determine the *COV*s of velocity and tracer gas for several different flow arrangements. First, as a baseline, measurements were made of the *COV*s at various downstream distances in a 305 mm × 305 mm (1 ft × 1 ft) straight square duct. Next, mixing elements were placed upstream of the straight square duct and upstream of a straight rectangular duct, 914 mm wide × 305 mm high (3 ft × 1 ft). The effect of the mixing elements on the *COV*s was evaluated in straight ducts following the elements, which is typically the location where a sampling station would be located. The square and rectangular ducts were fabricated from 19 mm thick insulating sheathing, a semi-rigid polyisocyanurate foam board insulation with aluminum foil facing on both sides (TUFF-R®, Dow Chemical Company, Houston, TX).

Although one of the ANSI mixing criteria deals with the *COV* of 10 μm AD aerosol particles, tests were not conducted with particles. For our test conditions, the behavior of the 10 μm AD particles would similar to that of the tracer gas. However, for situations where either a characteristic dimension of the duct is on the order of a few percent of the particle stopping distance or the dimensionless parameter, V*tL/UH* , is on the order of a few percent, special attention should be given to aerosol mixing. Here, *Vt* is gravitational sedimentation velocity. For the present study the stopping distance of 10 μm AD particles was less than about 2 mm, and the parameter V*tL/UH* was on the order of 1%.

Pressure drop across the mixing elements was measured to provide information so users can estimate the energy loss needed to provide the mixing. The data are reduced to

a pressure coefficient, so the energy losses of one element can be compared with that of another.

2.2.2. Tests of *COV*s in a Straight Square Duct

Figure 1 shows the apparatus use for testing mixing in a straight duct. The airflow from a pressure blower was passed through two sets of flow straighteners (6 mm diameter soda straws). The straighteners eliminated flow swirl and large scale eddies before the flow entered the region of the straight duct where velocity and tracer gas measurements were made. The blower was driven by a variable frequency controller that allowed a range of flowrates from 10 to 76 m³/min (350 to 2700 cfm) to be achieved.

For tests involving tracer gas, a small flow of dilute sulfur hexafluoride (SF6) was introduced into the bulk flow at a distance of 1 hydraulic diameter (D_H) downstream from the exit plane of the second set (relative to the pressure blower location) of straighteners. The sulfur hexafluoride was injected at flowrates and initial concentrations that would provide spatial average concentrations of approximately 5 ppb in the duct. The tracer gas was injected at five different locations across the duct cross section -- at the center, and at 25% of a hydraulic diameter from each of the four corners.

Concentration of the tracer gas was measured at the appropriate traverse points on a 16 point EPA Method 1 grid at various downstream sampling locations. For the straight duct, the downstream distance (L / D_H) is measured from the gas injection location. Concentration was quantified with a gas chromatograph (Model 101, Lagus Applied Technology, Inc., San Diego, CA). Samples of air (60 mL) were extracted at each

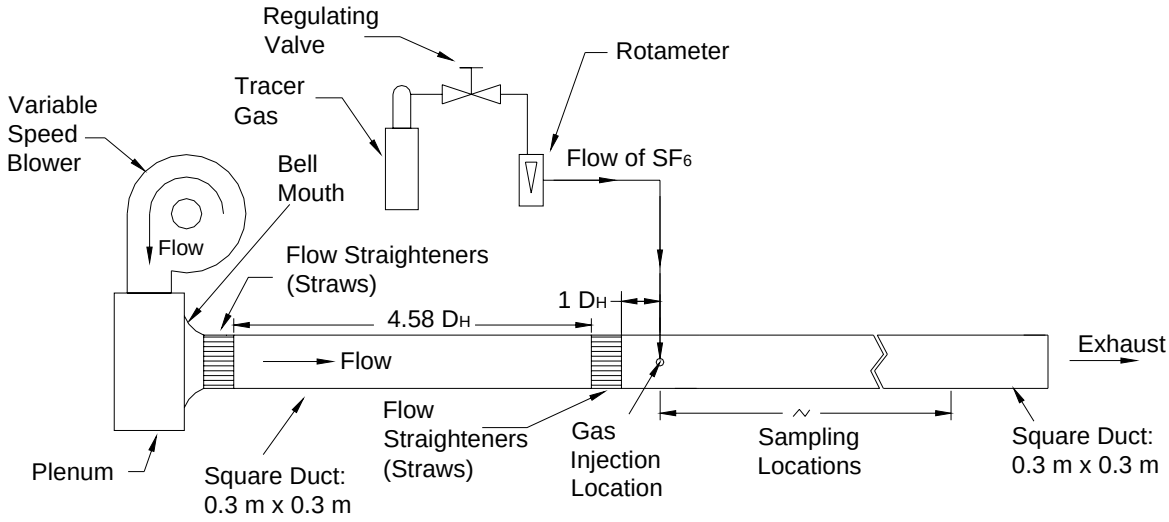

Figure 1. Arrangement Used to Test the Square Duct with No Mixing Element.

traverse point with hypodermic syringes, the syringes were capped to prevent leakage, and subsequently the samples were injected into the gas chromatograph. Velocity measurements were taken at the Method 1 traverse points with a thermal anemometer (Model 8355, TSI Inc., St. Paul, MN). Measurements of both tracer gas and velocity were made at all 16 points of an EPA Method 1 grid, and the calculations of the *COV*s are based on use of all 16 points.

Results from the straight duct tests were compared with those of previous tests with circular straight ducts (Anand et al., 2003) where the experiments had been conducted with a 152 mm (6 inch) diameter Schedule 40 PVC straight pipe. They used the center 12 points of a 16 point EPA Method 1 grid, which encompass 75% of the duct area and thereby meets the ANSI requirement of testing over at least the center 2/3 of the

duct area, whereas in the present study with a square duct we used all 16 points of an EPA Method 1 grid.

2.2.3. Tests with Mixing Elements Upstream of a Straight Duct

Mixing elements, e.g. 90° bends, were placed in the square and rectangular ductwork at a distance of 1 hydraulic duct diameter downstream from the tracer gas injection location. Several configurations of mixing elements were employed; namely, a 90° mitered bend (Figure 2), a 90° mitered bend with internal turning vanes (Figure 3), two 90° mitered bends in series with a U-shape (Figure 4), and two 90° mitered bends in series in an S-shape (Figure 5). Protocols for gas injection and sampling, and velocity measurements were the same as was used in the tests of the square duct with no mixing

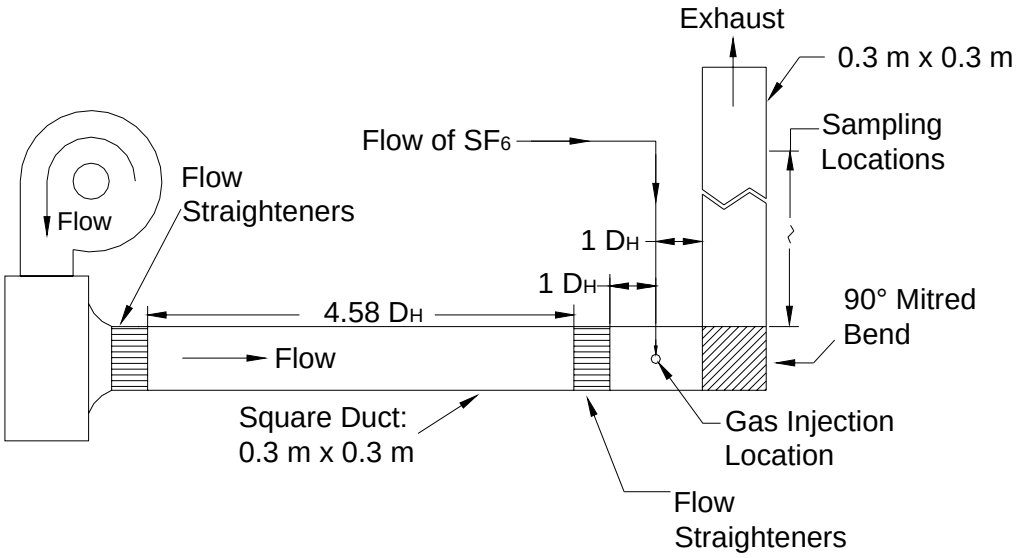

Figure 2. Arrangement Used to Test Straight Duct Preceded by a 90° Bend Mixing Element. Layout is Shown with a Square Duct; However, Tests Were Also Conducted with a 0.3 m High (into the paper) × 0.91 m Wide Rectangular Duct with 4.0 D_H Distance between Straighteners.

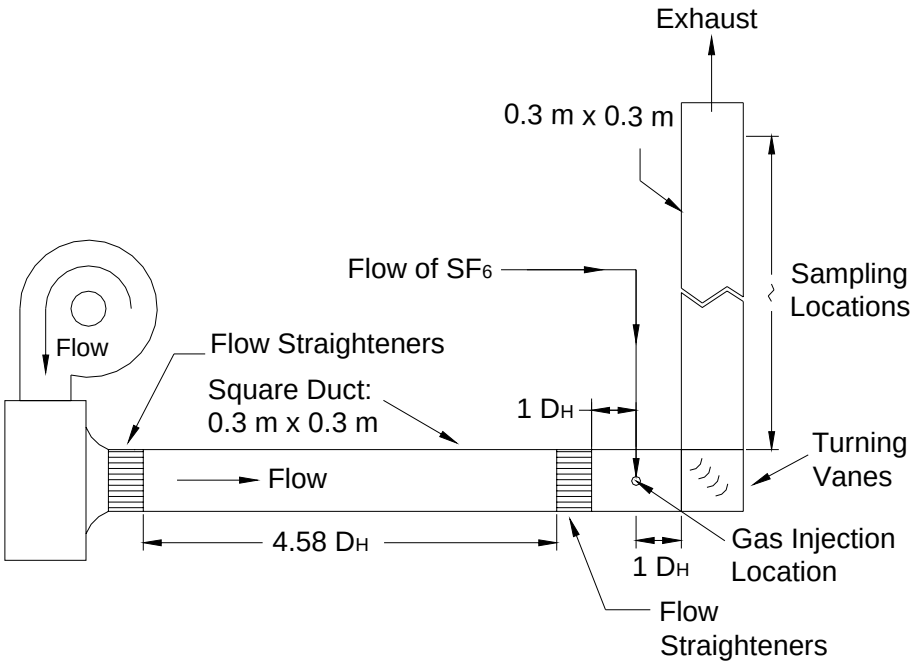

Figure 3. Arrangement Used to Test the Effect of Turning Vanes in a Mitered 90° Bend.

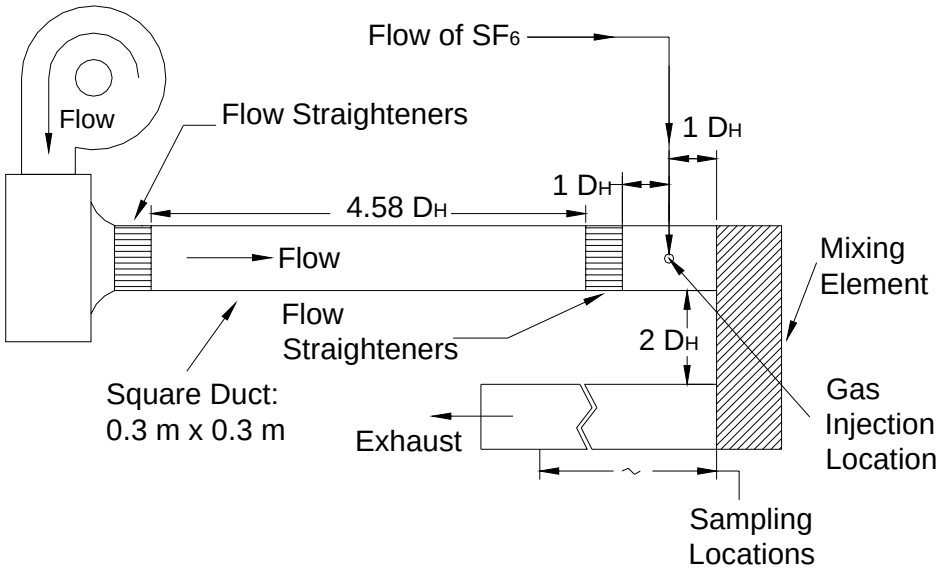

Figure 4. Experimental Setup Used to Test U-type Double Bends.

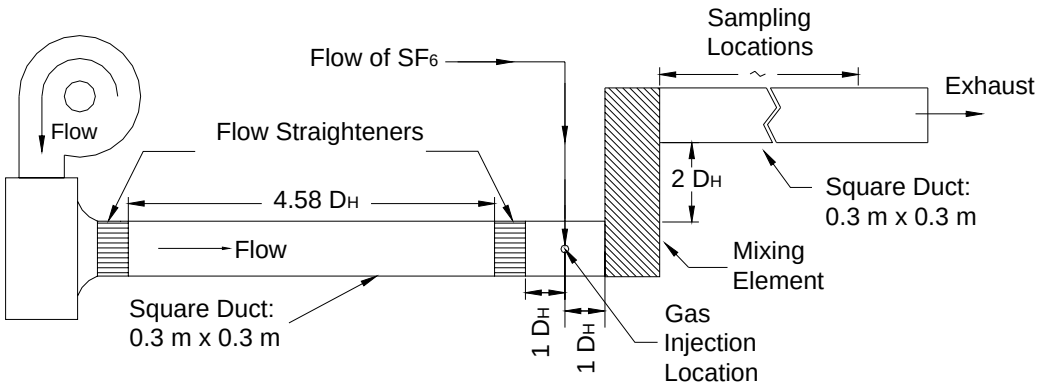

Figure 5. Experimental Setup Used to Test S-type Double Bends.

element. The zero point for downstream distance for these experiments was taken as the exit plane of the mixing element (see, for example, Figure 2). To make a direct comparison of tracer gas *COV* with the data from the straight ducting with no mixing element, a value of $L/D_H = 1$ must be added to the straight duct results. This takes into account the fact that the gas release in the mixing element study has an opportunity to slightly diffuse in the 1 diameter of straight ducting just upstream of the mixing element. Setting the zero point at the exit plane of a mixing element allows comparison of results with those of other studies (e.g., McFarland et al. 1999b) with mixing elements followed by circular ducts; whereas, setting the zero point for the straight duct tests (no mixing elements) allows comparison with previous tests with circular straight ducts (Anand et al., 2003).

Pressure drop across the mixing elements was measured through the use of taps located 1 diameter (D_H) upstream of the entrance port and 1 D_H downstream of the exit port of a mixing element. Four pressure taps at both the entrance and exit port of a mixing element were used to obtain an average pressure. Pressure loss is characterized with a pressure loss coefficient, *K*, which is defined as:

$$K = \frac{\Delta P}{\rho U^2 / 2} \qquad (6)$$

where: ΔP is the pressure differential across the mixing element; ρ is the air density; and, *U* is the mean speed of the flow through the duct cross sectional area.

2.3. RESULTS AND DISCUSSION

2.3.1. Straight Square Duct with No Mixing Element

Figure 6 shows the velocity and tracer gas *COV*s as a function of downstream distance in the straight duct with no mixing elements. Because there are flow straighteners upstream of the location where $L / D_H = 0$ in square ducts, the velocity *COV* is small – only about 6% and that value is independent of downstream distance. The flow straighteners uniformize the initial velocity profile and because the flow is turbulent, the asymptotic profile will be relatively flat. Comparative velocity results for a circular pipe (Anand et al, 2003) show a velocity *COV* of 2% at $L / D_H = 1$ and a gradual increase with distance towards a value of 7%, which is the typical *COV* for fully developed turbulent flow in a circular pipe. Their low initial value is a result of the use of a screen at the pipe inlet that uniformized the velocity profile to a greater extend than the straighteners of the present study.

Because SF6 is introduced at a discrete point in the flow, the tracer gas *COV* will

have a very high initial value that will gradually decrease with downstream distance as a consequence of the turbulent mixing process. The tracer gas *COV* data shown in Figure 6b are associated with a release of SF6 at the center of the duct. With reference to Figure 6b, even at a downstream distance of 19 duct diameters, the tracer gas *COV*s for square and circular ducts (Anand et al. 2003) are still 143% and 147%, respectively. Clearly, very long distances are needed in straight ducts with no preceding mixing elements in order to reach the ANSI maximum permissible value of 20%.

2.3.2. Square and Rectangular Ducts Preceded by a 90° Mitered Bend

2.3.2.1. *Effect of Reynolds Number*

Tests were conducted to determine if Reynolds number had any effect on the mixing downstream of the mixing element (90° bend) in the square and rectangular (3:1 aspect ratio) ducts, where the Reynolds number is defined as:

$$\mathrm{Re} = \frac{\rho U D_H}{\eta} \qquad (7)$$

Here, η is the dynamic viscosity of the air. Because the values of *Re* for tests with the square and rectangular ducts varied from 20,000 to 130,000, which is considerably greater than the value of 3200 that is taken as the upper limit for onset of turbulent flow in a circular duct (Fox and McDonald, 2001), the flow for these tests is turbulent. To determine if *Re* has an affect on mixing, the value of *Re* was varied by changing the velocity. Measurements in the square and the rectangular duct for the velocity and tracer gas *COV*s were made at downstream distances from the exit planes of the mixing elements of 9.5 and 11 hydraulic diameters, respectively.

With reference to Figure 7a, the velocity profiles in both ducts show little

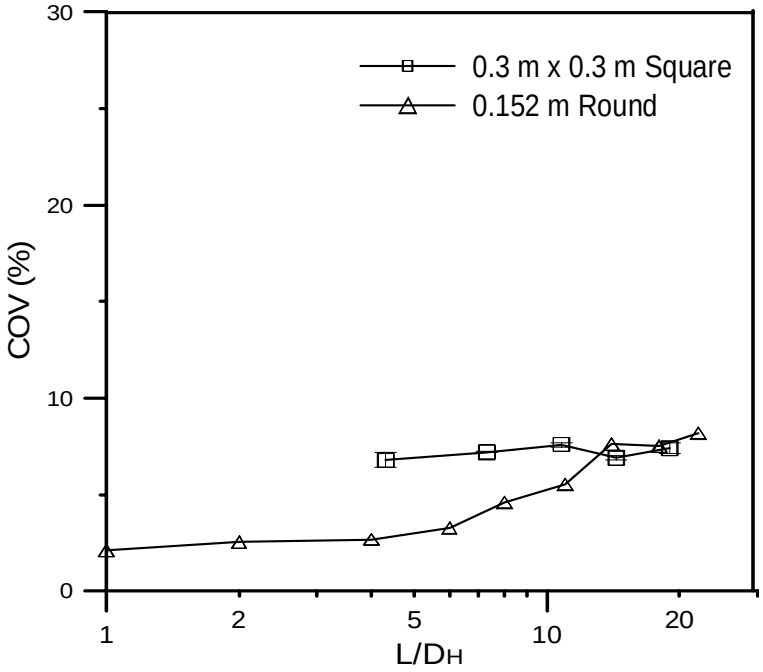

a)

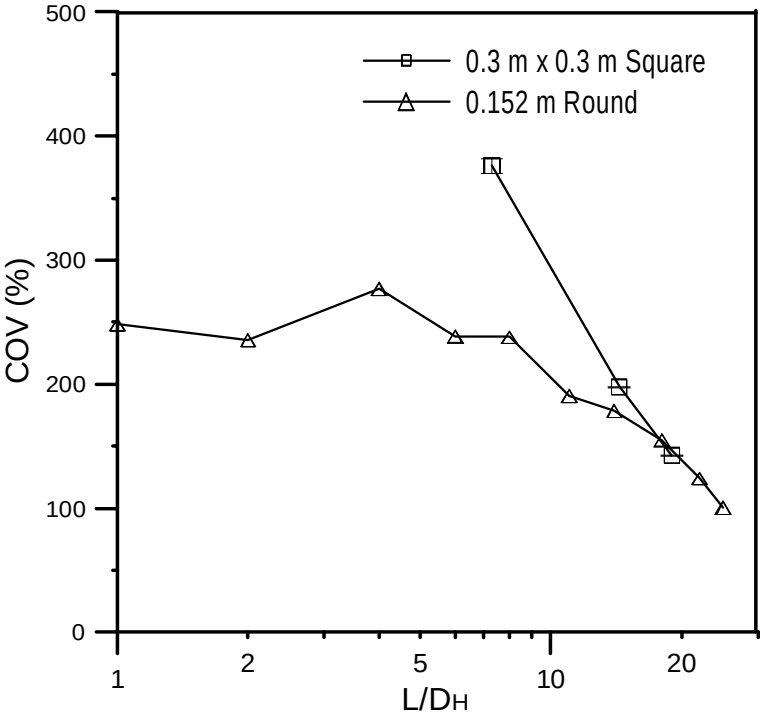

b)

Figure 6. *COV* of as a Function of Downstream Distance (L/*DH*) in a Straight Square Duct. a)Velocity. b) Tracer Gas (Release at Center of Duct). Comparative Data for a Circular Duct (Anand et al.,2003) Are Also Shown. The Flow Reynolds Numbers Were 127,000 for the Square Duct and between 5,000 and 16,000 for the Circular Duct.

dependence on Reynolds number over the range of Reynolds numbers tested. There is a slight tendency for the *COV*s to be lower at the higher Reynolds numbers, which is a phenomenon that has been previously noted and discussed (McFarland et al., 1999a). The *COV*s of the rectangular duct are significantly higher than those of the square duct – at a Reynolds number of 10^5 , the value at the distance of 11 diameters downstream from a 90° bend for the rectangular duct was 23% while that at 9.5 diameters downstream from a 90° bend in the square duct, the tracer gas *COV* was 6%. These results suggest that even at a distance of 10 diameters downstream from a 90° bend, the turbulent eddies in a wide duct do not have sufficient opportunity to effectively transfer momentum from one side of the duct to the other and thereby uniformize the velocity profile.

The *COV*s of tracer gas concentration (Figure 7b) show only a small Reynolds number effect for the square duct over the range of $25{,}000 \leq Re \leq 150{,}000$. However, the tracer gas *COV*s in the rectangular duct are affected by Reynolds number for $Re \leq 50{,}000$. The tracer gas was injected into the center of both ducts at the injection locations. For the rectangular duct, at a Reynolds number of 25,000, the tracer gas *COV* was 46% and at a Reynolds number of 100,000, the *COV* was 21%. In contrast, for the square duct, the *COV* was 22% at a Reynolds number of 28,500 and 16% at a Reynolds number of 100,000. These results suggest that a higher aspect ratio may cause an increase in the value of the lowest Reynolds number at which geometric similarity dominates mixing.

2.3.2.2. *COVs Downstream of a 90° Bend*

Tests were conducted to characterize the effect of downstream distance on the velocity and tracer gas *COV*s for both the square and rectangular duct. Reynolds numbers were 127,000 and 117,000 for the square and rectangular ducts, respectively. The tracer

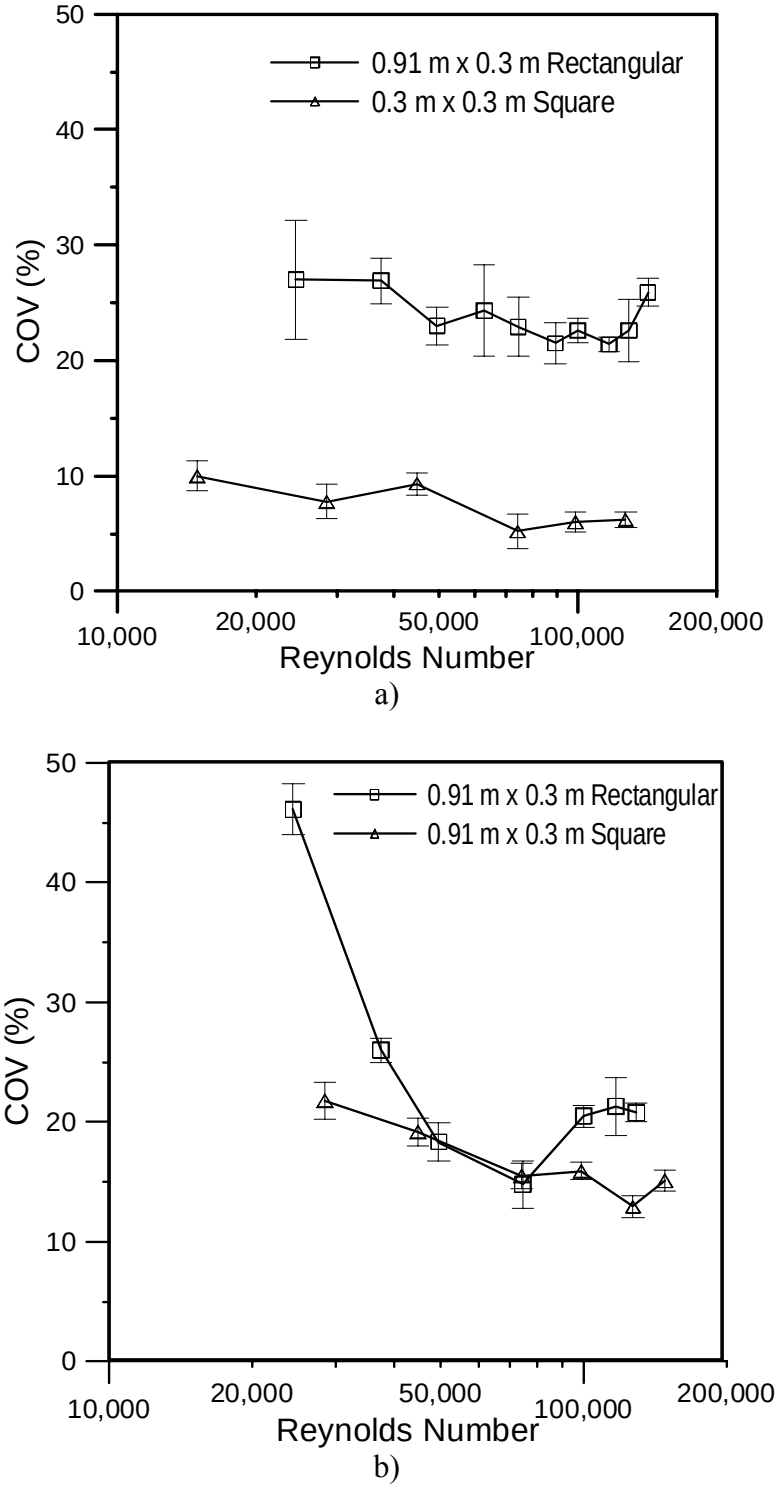

Figure 7. *COV*s as a Function of Reynolds Number for Rectangular (Aspect Ratio of 3:1) and Square Ducts Preceded by 90° Mitred Bends. Sampling Locations were at 9.5 and 11 Hydraulic Diameters from the Exit Plane of a Bend for the Square and the Rectangular Duct, Respectively. a) Velocity. b) Tracer Gas (Release at Center of Duct).

gas injection locations were at the centers of the ducts.

The results for the velocity *COV*s, Figure 8a, show that at a distance of 9 hydraulic diameters, the velocity *COV* was 6.4% for the square duct and 29% for the rectangular duct. Also, the mixing of tracer gas was better in the square than in the rectangular duct, Figure 8b. At a distance of 9.5 hydraulic diameters, the *COV* for the square duct was 12.9% whereas that for the rectangular duct was 27%. Even at the $L / D_H = 11$, the highest value at which tests were conducted, the *COV*s for the rectangular ducts still have significant slopes, so additional ducting would further improve the mixing.

2.3.2.3. *Effect of Location of Gas Injection Point*

The ANSI standard requires that for a noncircular duct, the tracer gas must be released at the center of the duct and within 25% of a hydraulic diameter from each corner. Figures 9a and 9b show the results when SF6 was released at the corners and center of the square and rectangular duct setups, respectively. When SF6 was released at the inside of a bend, the *COV*s are higher than when it was released at the outside of a bend. Release of the tracer gas at the center of the duct produces low *COV* values, particularly in the case of the rectangular duct.

2.3.2.4. *Comparison of Mixing in Square and Circular Ducts*

McFarland et al. (1999b) reported on the *COV*s for tracer gas and velocity in circular ducts preceded by 90° bends, and their results are compared with those for the square duct in Figure 10. The square duct had a mitred bend whereas the circular duct of McFarland et al. had a smooth bend with a curvature ratio (radius of the bend to the tube radius) of 2.0. For shorter downstream distances, the mixing in the circular duct is

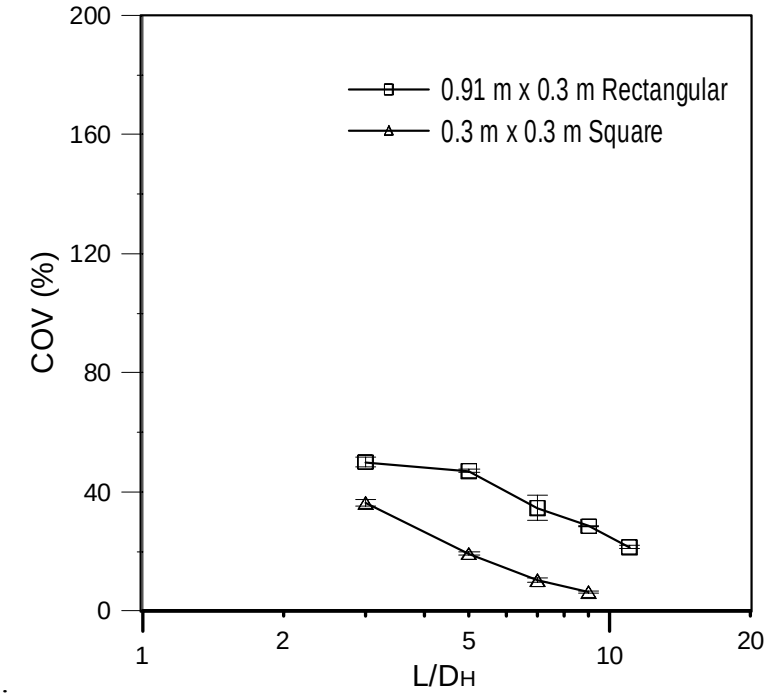

a)

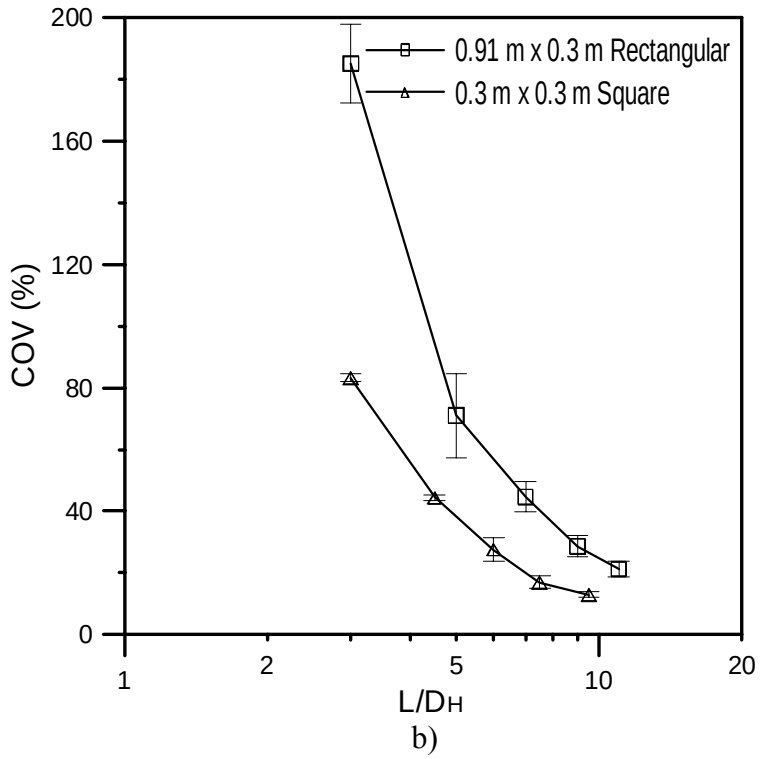

b)

Figure 8. *COV*s as a Function of Sampling Location (L/D_H) for a Single 90° Mitred Bend. The Flow Reynolds Numbers Were 127,000 for the Square Duct and 117,000 for the 3:1 Aspect Ratio Rectangular Duct. a) Velocity. b) Tracer Gas (Release at Center of Duct).

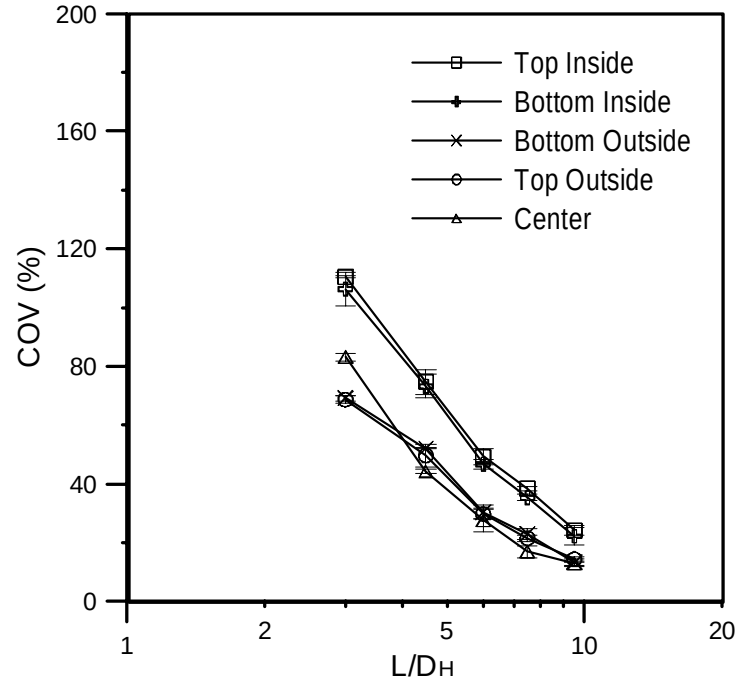

a) Reynolds Number: 127,000

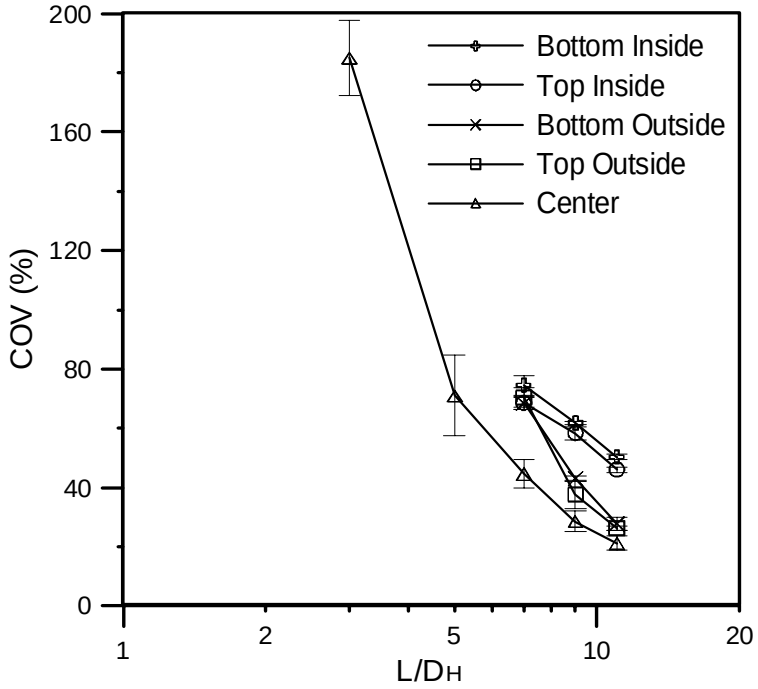

b) Reynolds Number: 117,000

Figure 9. Effect of Release Point on *COV*s of SF_6 Concentration as a Function of Sampling Location (L/D_H) Downstream of a 90° Mitred Bend. a) Square Duct. b) Rectangular Duct (3:1 Aspect Ratio).

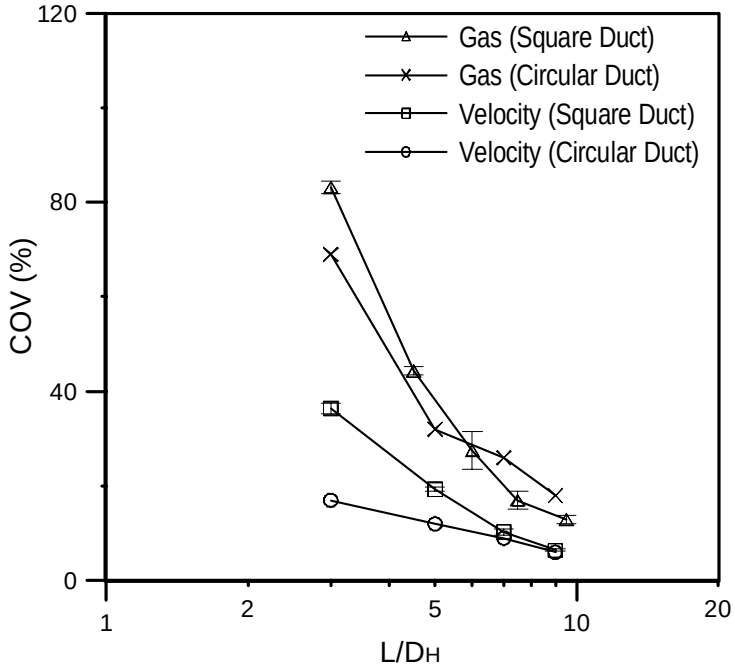

Figure 10. Comparison of Velocity and Tracer Gas (Release at Center of Duct) *COV*s Downstream of a Smooth Bend in a Circular Duct (McFarland et al. 1999b) and a Mitred Bend in a Square Duct. The Flow Reynolds Numbers Were 127,000 for the Square Duct and 64,000~300,000 for the Circular Duct.

somewhat more effective than that in the square duct, e.g., at distance of 3 hydraulic diameters downstream from the bend the gas *COV* for the circular duct is 69% while that for the square duct is 83%. This is probably due to the fact that twin secondary vortices are setup in the central area of the circular duct as the flow travels through the bend, and these vortices enhance the mixing. However, for downstream distances greater than about 6 hydraulic diameters, the *COV*s are comparable.

2.3.2.5. *Effect of Turning Vanes*

A single 90° square mitred bend with turning vanes was tested to simulate practical situations, where turning vanes are often used in the mitered bends to reduce pressure losses. Results, Figure 11, show that for the situation of a center release of tracer gas, the *COV* is 50.9% at 9.5 duct diameters downstream of the 90° square bend with

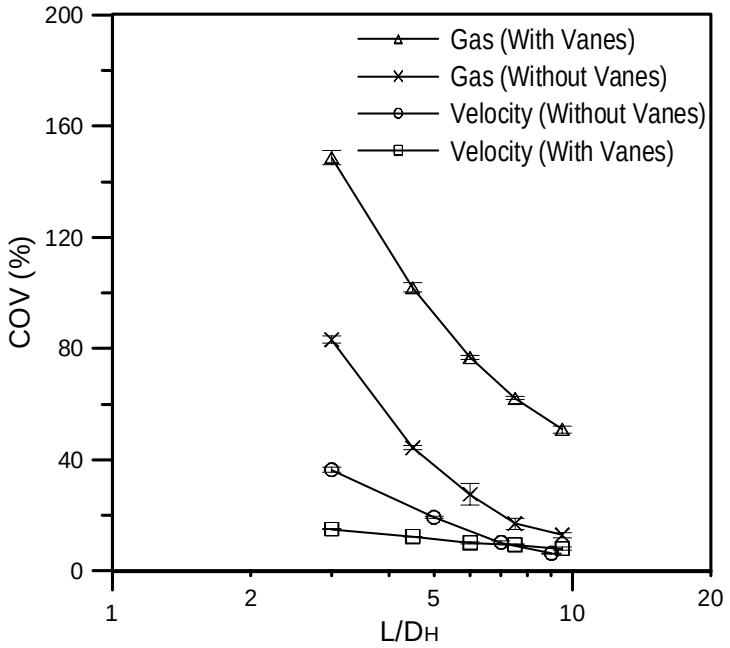

Figure 11. Comparison of the Tracer Gas (Release at Center of Duct) and Velocity *COV*s for Downstream of a 90° Bend with and without Turning Vanes. Reynolds Number: 127,000.

turning vanes, whereas it is 12.9% for the center release case with a mitred bend with no turning vanes. Tracer gas releases in the four corners of the duct preceded by the bend with turning vanes yielded even higher *COV*s than the center release (Figure 12).

2.3.3. Square and Circular Ducts Preceded by Multiple Bends

2.3.3.1. *U-Shaped Bends*

A comparison of the tracer gas *COV*s created with center releases upstream of a mitred bend in a square duct (present study) and a smooth bend in a circular tube (McFarland et al., 1999b), is shown in Figure 13. Quite similar results are obtained for the two duct cross sections, even though better mixing was obtained with a single circular duct than with a single square duct. For the square duct, at a distance of 6 diameters the tracer gas *COV* is 30%, whereas at that same distance the *COV* for a circular duct with a center release is 31%.

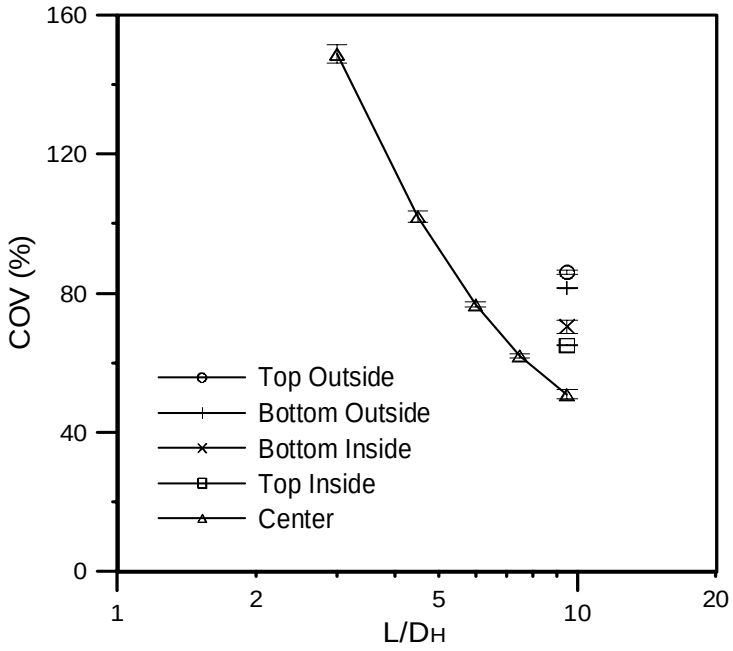

Figure 12. Effect of Release Location on Tracer Gas *COV*s at a Distance of 10 Hydraulic Diameters from a 90° Mitred Bend with Turning Vanes. Reynolds Number: 127,000.

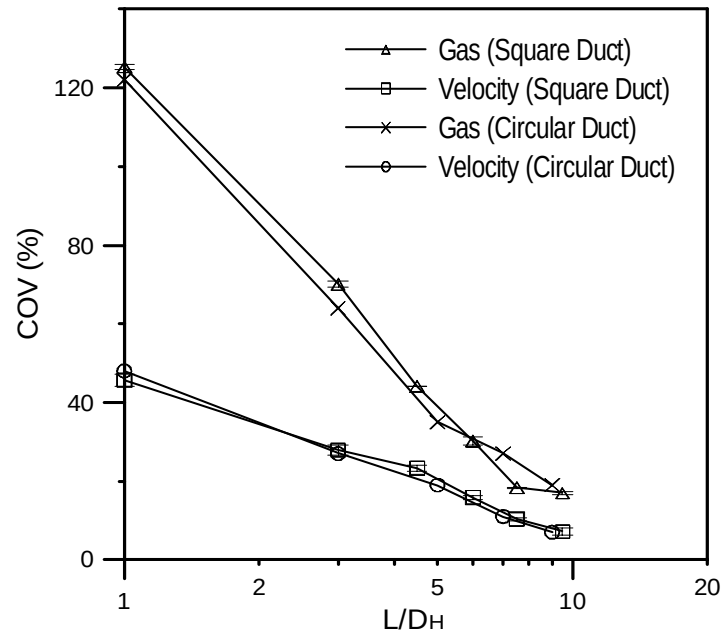

Figure 13. *COV*s of SF6 Concentration (Release at Center of Duct and Velocity) Downstream of U-type Double Bends. Square Duct Cross Section with a Mitred Bend (Present Study) and Circular Cross Section with a Smooth Bend (McFarland et al. 1999b). The Flow Reynolds Numbers Were 127,000 for the Square Duct and 64,000~300,000 for the Circular Duct.

Figure 14 shows the effect of injection location on the *COV*s in the square duct, where it may be noted that at a distance of 3 diameters the highest *COV*s was associated with as center release. By the time the flow reaches the 6 diameter location, the mixing is approaching independence from the release location.

2.3.3.2. *S-Shaped Bends*

Hampl et al. (1986) noted that mixing elements comprised of two bend of circular cross section placed in an S-configuration produced much better mixing than either a single bend or two bends in a U-configuration. McFarland et al. (1999b) ascribed the enhanced mixing to the rotation of the vortices in the core of the circular bends being reversed in direction as the flow from the first bend travels into the second. The results of the present study, Figure 15, show that for the square duct, the *COV*s for tracer gas

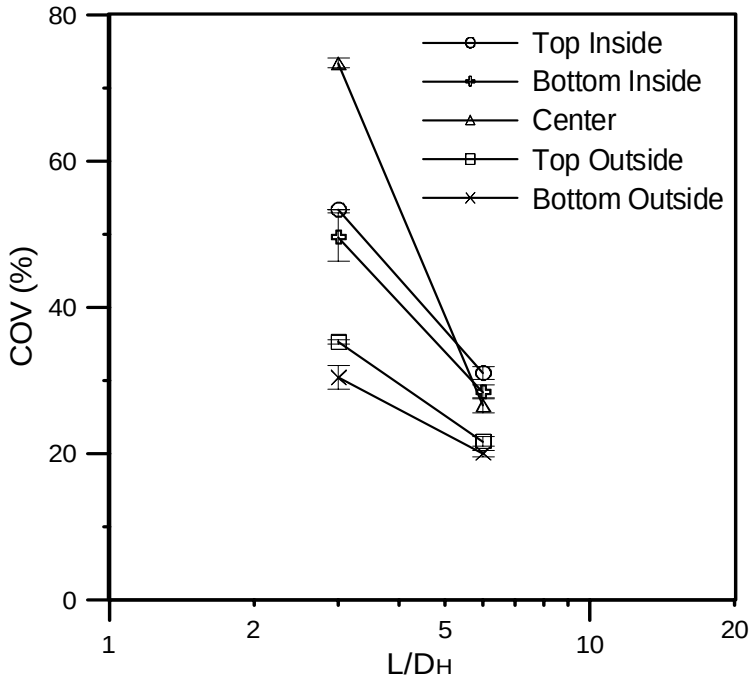

Figure 14. *COV*s of SF6 Concentration Downstream of a U-type Double Bend in Square Ducts for Various SF_6 Release Points. Reynolds Number: 127,000.

(center release) and velocity are 8% and 23.5%, respectively, at a distance of 4.5 diameters. If a sampling location were to be placed downstream of an S-configuration in a square duct, the velocity *COV* could easily be lowered by installing a set of flow straighteners at a distance ≥ 4.5 diameters from the mixing element, and then placing the inlet of the sampler approximately one diameter downstream of the exit plane of the straightener.

The results show that the gas *COV* for square duct is 5% at a distance of 6 diameters, which is somewhat better than the 12% value for mixing in the circular duct measured at the same location. Gupta (1999) showed that mixing in circular ducts could be improved by increasing separation distances between the two bends.

Tests were also conducted to determine the effect of release location on the *COV*s for tracer gas in the square duct. As shown in Figure 16, the highest *COV* values were associated with gas releases on the inside corners of the first bend. However, when the flow has traveled 6 diameters from the exit plane of the mixing element, the *COV*s are less than 8% regardless of release location.

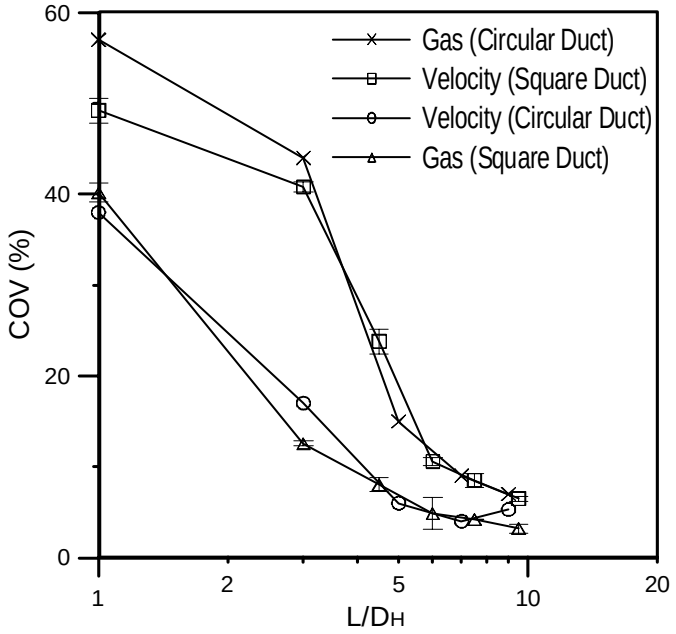

Figure 15. *COV* of SF_6 Concentration (Release at Center of Duct) and Velocity as a Function of L/D_H Downstream of S-type Double Bends in Square and Circular Ducts (McFarland et al. 1999b). The Flow Reynolds Numbers Were 127,000 for the Square Duct and 64,000~300,000 for the Circular Duct.

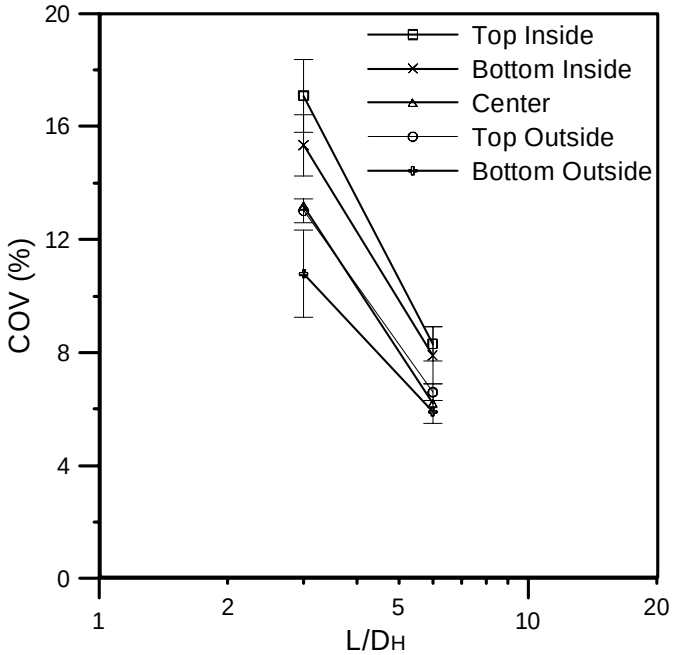

Figure 16. *COV*s of SF6 Concentration Downstream of an S-type Double Bend in Square Ducts for Various SF_6 Release Points. Reynolds Number: 127,000.

2.3.4. Pressure Loss across Mixing Elements

The results from pressure loss experiments are shown in Figure 17, where the pressure differential across the mixing element is shown as a function of Reynolds number based on hydraulic diameter. The pressure loss data have been converted to flow coefficients through use of Equation 6, and the results are given in Table 1. The data are compared with those of circular ducts (McFarland et al. 1999b), and the results show the losses in non-circular are greater that circular. For comparison, data from the literature on pressure losses across mitred bends (ASHRAE, 1989) are also shown.

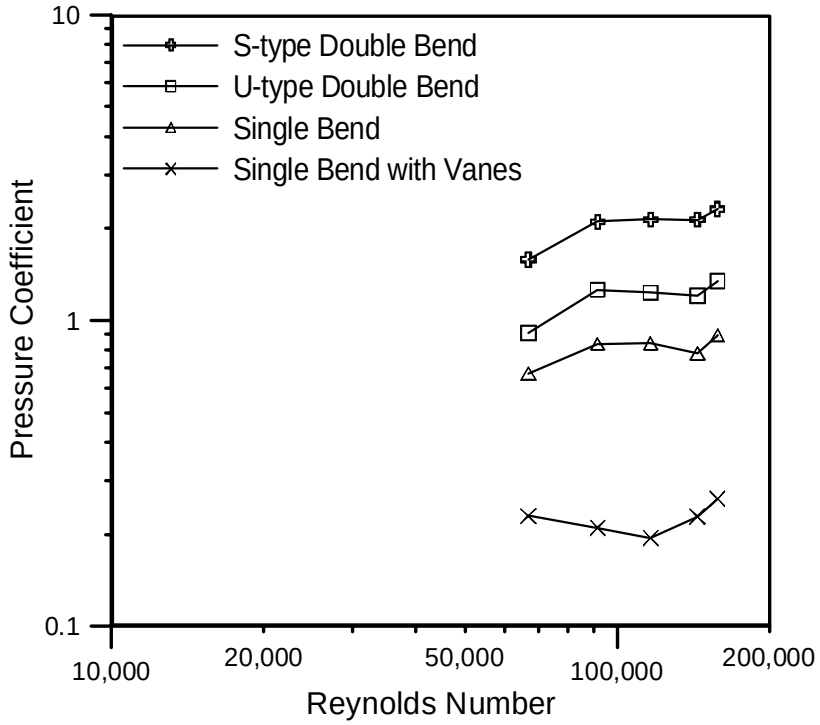

Figure 17. Pressure Coefficient Across Mixing Elements as a Function of Reynolds Number.

Table 1. Pressure Coefficients for Various Mixing Elements. All Bends Are Mitred Except the Circular Bends of McFarland et al. (1999b), Which Are Smooth with a Curvature Ratio of 2.0.

Configuration	Circular Duct (McFarland et al, 1999b)	Square Duct (Present Study)	Square Duct (ASHRAE, 1989)	Rectangular (3:1) Duct (Present Study)	Rectangular (3:1) Duct (ASHRAE, 1989)
90° bend	0.6	0.84	1.25	1.1	1.35
90° bend with turning vanes[1]	-	0.23	0.18	-	-
Double bend : U-arrangement	1	1.26	-	-	-
Double bend : S-arrangement	1.7	2.20	3.38	-	3.69

[1] Four turning vanes were used in the duct of the study and seven for the ASHRAE data.

2.4. ERROR CONSIDERATIONS

Measurements in this study were primarily based on use of a thermal anemometer and a gas chromatograph with an electron capture detector. The uncertainties associated with an anemometer reading (when the air temperature is within the range of 40 to 150°F) are quoted by the manufacturer as:

- Range: 0.15 to 2.5 m/s: ± 2.5% of reading ± 0.01 m/s.
- Range: 2.5 to 10.3 m/s: ± 2.5% of reading ± 0.1 m/s.

The relative uncertainty in an anemometer reading can be estimated by combining the two quoted uncertainties coupled with an assumption of statistical independence. For example, at a velocity of 5 m/s, the relative uncertainty in a velocity measurement,

$e(U)/U$, is:

$$e(U)/U = \sqrt{0.025^2 + (0.1/5)^2} = 0.032$$

i.e., the relative error would be 3.2%.

The manufacturer of the chromatograph quotes the uncertainty of a reading as:

- Range: 0.5 to 21 ppb (parts per billion): ± 4% of reading
- Range: 0.18 to 50 ppb: ± 10% of reading
- Range: near 5 ppb: 0% of reading

The range of velocity in this research was between 0.77 and 7.2 m/s and the range in tracer gas concentration was from 0.4 to 25 ppb. This infers the relative uncertainty in velocity determinations was ≤3% and that for tracer gas was ≤10%.

To check the reproducibility of the data, 16 measurements of both velocity and SF6 concentration were performed at 9.5 duct diameters downstream from a single 90° bend in the square duct setup. The sampling points were at the center of the duct. The relative error (standard deviation/mean) of the velocity measurements was 3.2%, and the relative error of the concentration measurements was 2.9%.

The results for the *COV*s obtained in this study are based on calculations from at least triplicate tests at each condition. Error bars shown in the figures represent ± 1 standard deviation about the mean value. The average error bar (standard deviation) of all velocity *COV*s was 1.1% and that of all tracer gas *COV*s was 1.7%.

CHAPTER III

DESIGN OF AN INLET FOR AMBIENT AEROSOL

3.1. PREFACE

3.1.1. General

Biological or chemical weapons can be released into the ambient environment; therefore, they must be detected as quickly as possible to allow immediate treatment or evacuation. For troops in the field, rapid detection of biological agents is dependent upon acquisition of samples that do not underestimate the agent concentration. To accomplish this, reliable aerosol inlets are needed. An inlet is the device through which samples from the ambient environment are extracted. The effectiveness of an inlet is dependent upon both the size of the aerosol and the wind speed in the ambient environment. Inlets need to prevent precipitation, debris, and insects from entering a bioaerosol sampler while also permitting the penetration of aerosol particles in the size range of interest (1 to 10 μm aerodynamic diameter). Here, the aerodynamic diameter *(*AD*)* is the diameter of the spherical particle with a density of 1000 kg/m³ that has the same settling velocity as the particle (Hinds, 1999).

3.1.2. Objectives

The objective of this study was to develop improved inlets for a Battelle bioaerosol sampling system. The current Battelle inlets are a 780 L/min main unit, which operated on a part-time basis and a 90 L/min unit that is operated continuously. The 780 L/min unit (Figure 18a) features a flat top plate and an internal fractionator (impactor) that precludes entry of large particles. The impactor jet has a diameter of 4.9 cm (1.93 inch) and the inlet has an intake gap of 1.3 cm (0.5 inch). For comparison, an inlet developed in this study to perform the tasks of the Battelle 780 L/min unit, the ALL WEATHER INLET 780 L/min (AWI-780) device is shown in Figure 18b. The 780 L/min sampler of the Battelle system is actuated only when a detector fed by the Massachusetts Institute of Technology (MIT) inlet (Figure 19) indicates an anomalous response. Both the Battelle and MIT inlets should be able to prevent insects, debris, precipitation, and carryover or re-entrainment of particles larger then 20 μm, etc. from entering the detection systems. In addition, the penetration of the inlets should be at least equal to or higher than the penetration of the existing inlets over the size range of interest (1 to 10 μm aerodynamic diameter, AD). The 0.0015 m^3/s (90 L/min) trigger unit should also have a high penetration of aerosol particles with sizes as large as 10 μm AD.

The Battelle 780 L/min inlet was tested by Drs. Haglund and Chandra at the Aerosol Technology Laboratory, Texas A&M University and Figure 20 shows that they determined the Battelle inlet has about a 9 μm AD cutpoint.

Detailed objectives for this study are development of:

1. An enhanced AWI-780, which operates at a flowrate of 0.013 m^3/s (780 L/min), should have a 10 μm AD cutpoint.

2. An AWI-90, which operates at a flowrate of 0.0015 m³/s (90 L/min), should be developed for use on the "trigger" MIT inlet of the Battelle. The configuration of the AWI-90 is the same as that of the AWI-780, but the size is one-third of the AWI-780.
3. The best screen should be determined so that it effectively blocks insects, yet allows particles to penetrate through it in the size range of interest (1 to 10 μm AD)
4. The enhanced AWI-780 and AWI-90 inlets will be tested at different wind speeds - 2, 8, and 24 km/h (U.S. EPA, 1999). Penetration of an acceptable inlet should not be greatly affected by different wind speeds.

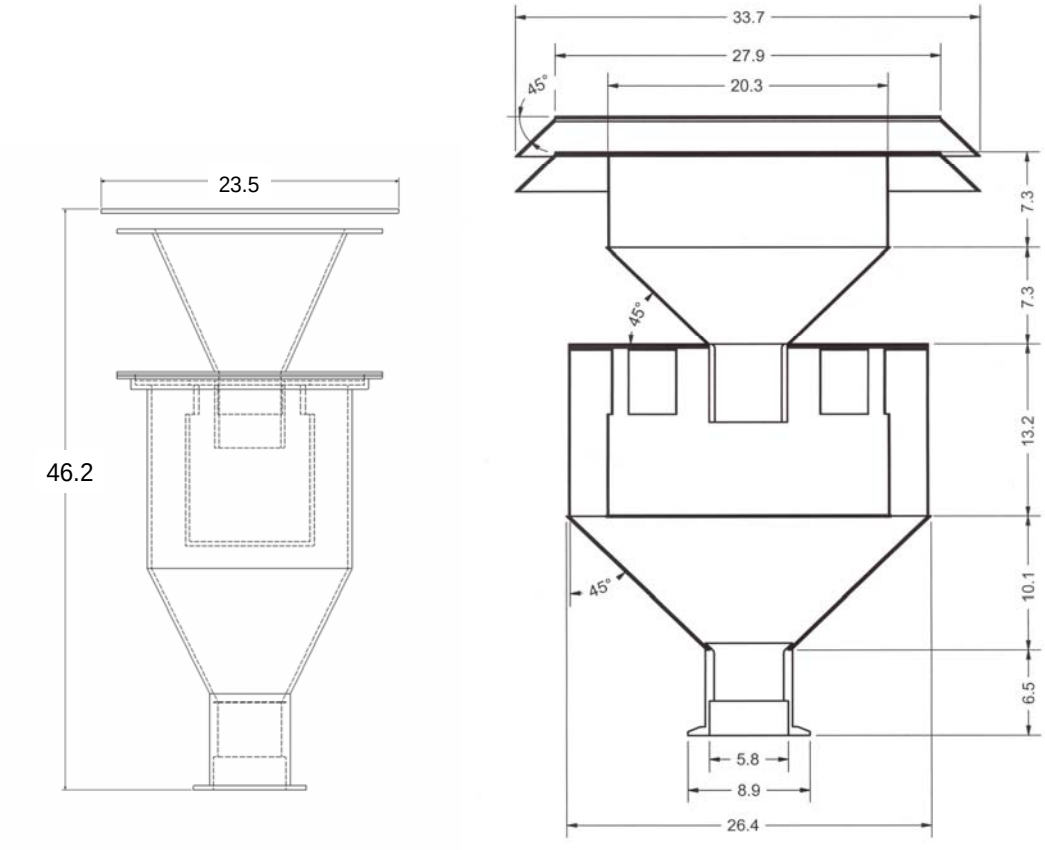

Figure 18. Schematic of Battelle Inlet (a) and the AWI-780 (b). All the Dimensions Are in Centimeters.

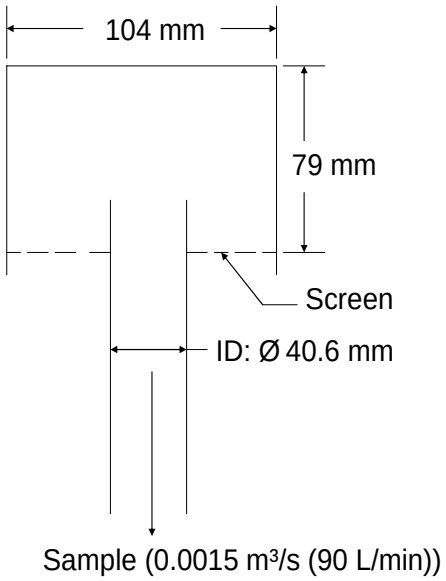

Figure 19. Schematic of the MIT Inlet.

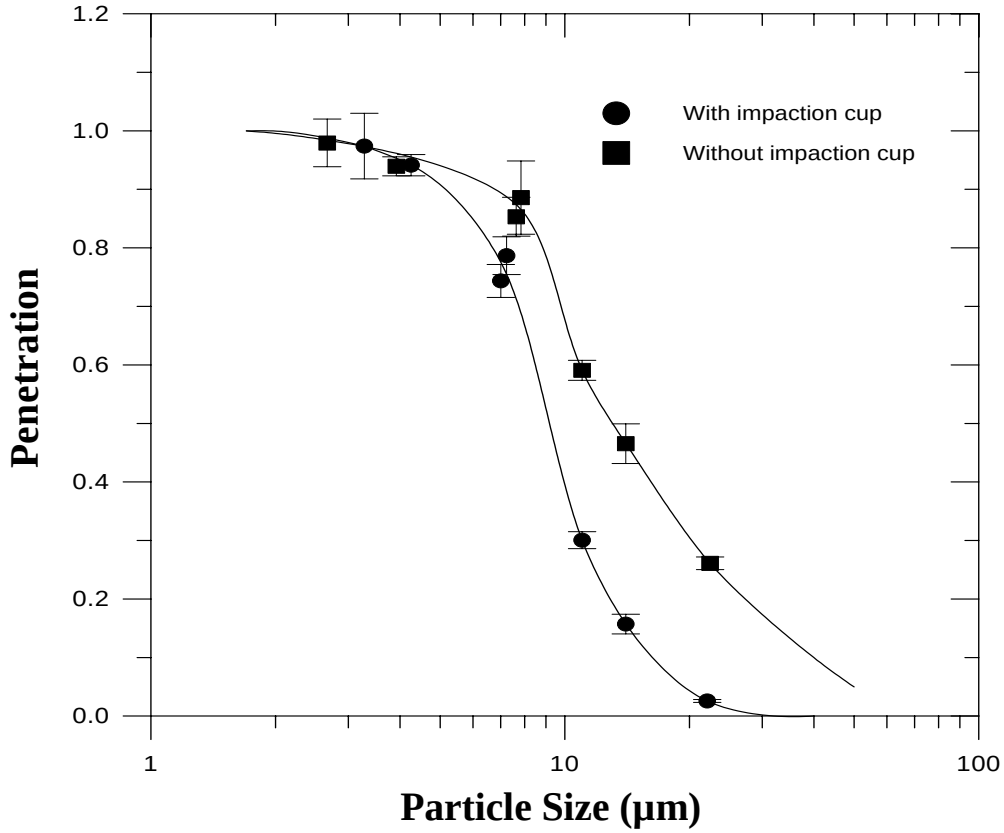

Figure 20. Penetration as a Function of Particle Size for Battelle Inlet. (Haglund and Chandra, 2000)

3.2. EXPERIMENTAL PROTOCOL

3.2.1. General

Two wind tunnels were used for testing inlets. A 0.61m × 0.61m (24"×24") system (Figure 21) was used initially to generate slow wind speeds such as 2, 4, and 8 km/h and a 0.86m (34") diameter wind tunnel (Figure 22) was subsequently used for wind speeds as high as 24 km/h. The velocity of air in the square wind tunnel was adjusted by varying the flow outlet area and the velocity in the round wind tunnel was adjusted by controlling the speed of the electric motor/fan of the wind tunnel using the variable frequency drive. The wind speed was measured using a thermal anemometer (Model 8355, TSI, Inc., Shoreview, MN) at nine traverse points in the square tunnel (0.61m×0.61m) and at 16 points in the round tunnel (0.86m diameter). The uniformity of the velocity profile at the test section, as represented by velocity *COV* was about 9% and Tables 2 and 3 show *COV*s of velocity and liquid particle that was determined from a mixing study for the round wind tunnel at the Aerosol Technology Laboratory of Texas A&M University. Because *COV*s for velocity at the test section were less than 4% for all wind conditions – 2, 8, and 24 km/h (Table 2), and *COV*s for particles were less than 4% for the main testing particle sizes -5, 10, and 15 μm at the wind speed of 8 km/h (Table 3), the wind tunnel deemed to be acceptable for aerosol testing. If a *COV* was ≥10%, we would consider the wind tunnel configuration to be unacceptable used for aerosol testing.

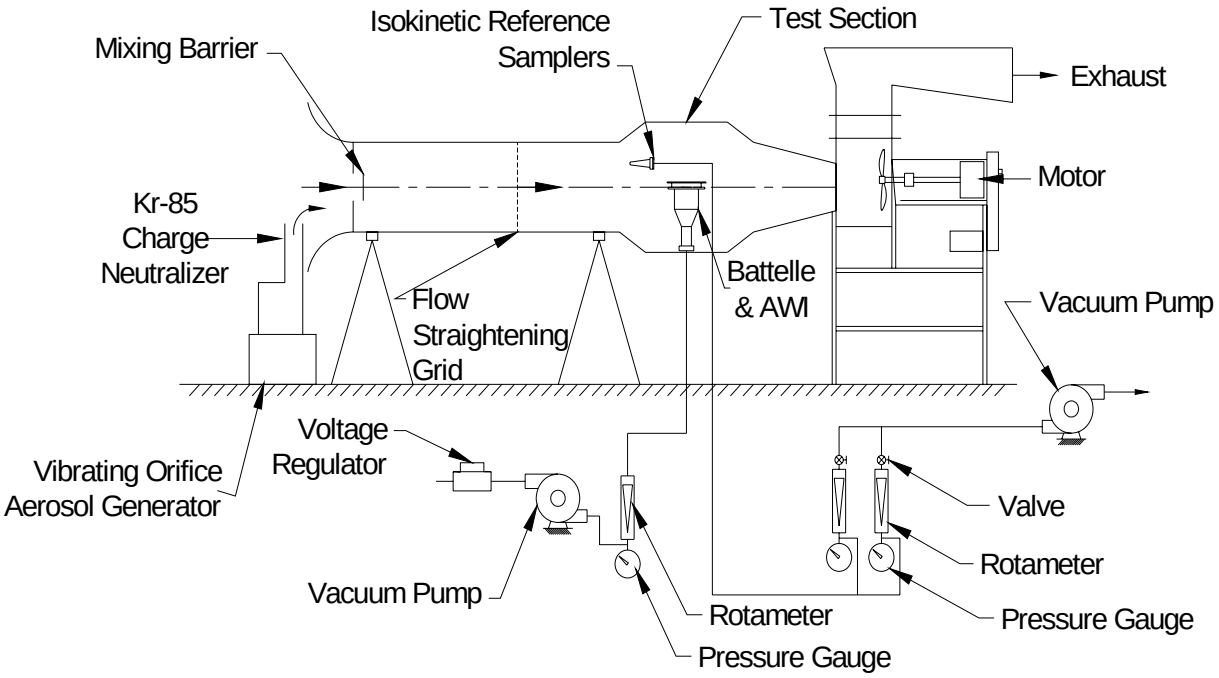

Figure 21. Schematic of the 0.6m × 0.6m Wind Tunnel.

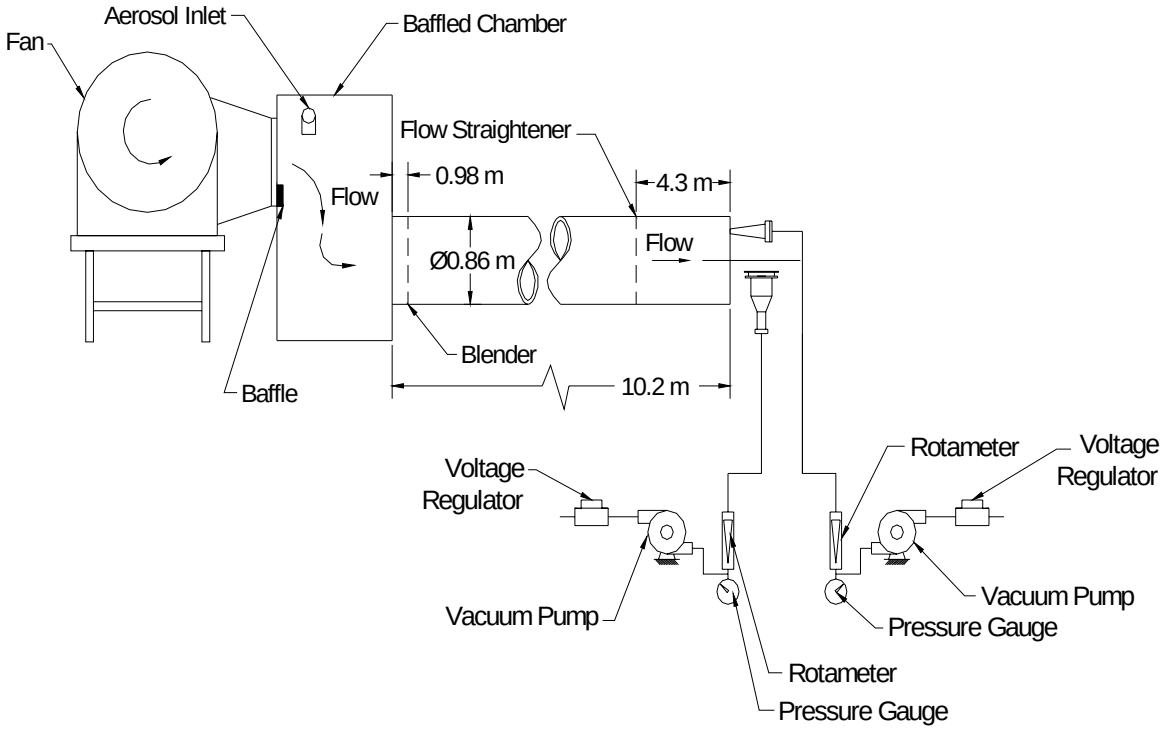

Figure 22. Schematic of 0.86m Diameter Wind Tunnel.

Table 2. Velocity COVs for 2, 8, and 24 km/h - 0.86 m Diameter Round Wind Tunnel.

Velocity, km/h	Velocity COV, %
2	3.8
8	3
24	2.7

Table 3. Particle COVs at the Wind Speed of 8 km/h - 0.86 m Diameter Round Wind Tunnel.

Particle size-µm	Particle COV, %
1 – 5	3.3
5 – 7	2.8
7 – 9	3
9 – 11	2.4
11 – 14	3.9

3.2.2. Inlet Designs

An AWI-780 inlet for bioaerosol sampling has been designed and tested. It features a rain roof to reduce the probability of rain and snow entering the sampler, it has an internal fractionator that precludes bounce or re-entrainment of large solid particles, and the intake gap of 1.3 cm (0.5 inch). In addition, an AWI-90, which is one-third scaled unit of the AWI-780, has been developed for use on the "trigger" of the Battelle sampler, which is called the Massachusetts Institute of Technology (MIT) inlet.

Because the cutpoints of the enhanced AWIs should be at least equal or higher than those of the Battelle and MIT inlets, a cutpoint management process is required. Particle size cutpoint is controlled by the cutpoint Stokes number and the particle

diameter, having 50% collection efficiency, d_{50} in terms of the values of Stk_{50}, can be calculated from:

$$d_{50}\sqrt{C_c} = \left[\frac{9\pi\eta D_j^{\ 3}(Stk_{50})}{4\rho_p Q}\right]^{1/2} \quad (8)$$

where, C_c is the slip correction factor, η is the viscosity of air, D_j is the jet diameter, Stk_{50} is the Stokes number that gives 50% collection efficiency, ρ_p is the density of the droplets, and Q is the jet flowrate (Hinds, 1999).

3.2.3. Test Procedures

A vibrating orifice aerosol generator (Model 3050, TSI, Inc., Shoreview, MN) was used to create liquid monodisperse aerosols (Berglund et al. 1973) from a mixture of oleic acid and sodium fluorescein dissolved in ethanol. The ethanol evaporates leaving the oleic acid tagged with sodium fluorescein, where the latter component is used for analysis of aerosol mass. After particle sizing, the monodisperse aerosol was introduced at the entrance of the wind tunnel. The 0.61 m × 0.61 m (24"×24") wind tunnel was only used to test the 780 L/min inlets and during the testing only the top chambers of the Battelle inlet and AWI-780 placed in the wind tunnel. During a test in the square wind tunnel, the test inlet and three 47 mm isokinetic probes were simultaneously operated at the test section, with the isokinetic probes serving the role of reference probes for establishing the concentration of aerosol in the wind tunnel. For tests with the 0.86 m (34") diameter wind tunnel, the whole assembly, including internal fractionator (Impaction Cup) and bottom chamber for both the Battelle inlet and AWI-780 placed in the airstream along with a 20.3 cm × 25.4 cm (8"×10") isokinetic reference probe. The

AWI-90 was tested by operating it simultaneously with two 47 mm isokinetic probes in the 0.86 m diameter wind tunnel.

Aerosol particles that penetrated through an inlet or an isokinetic probe were collected on a glass fiber filter (Type A/D or A/E glass, Pall Corporation, Ann Arbor, MI) and each filter was put in a storage container. To elute the sodium fluorescein tagged from the collection filter, a solution of 66.7% isopropyl alcohol and 33.3% distilled water was added to the filter. By using a fluorometer (Turner Quantech Digital Filter Fluorometer - Model 450, Barnstead International, Dubuque, IA), the amount of fluorescein collected on the filter was measured and the relative aerosol mass collected was calculated.

When calculating the relative concentration of the aerosol mass in the solution, the following formula was used:

$$C=\frac{RV}{tQ} \tag{9}$$

Where, C is the relative concentration, R is the numerical reading from a fluorometer (Turner Quantech Digital Filter Fluorometer - Model 450, Barnstead International, Dubuque, IA), V is solution volume, t is time for each test, and Q is flowrate. The penetration was calculated by using the following:

$$P=\frac{C_{inlet}}{C_{iso}} \tag{10}$$

where, C_{inlet} is the relative concentration of the aerosol mass, collected on the filter from an inlet and C_{iso} is the relative concentration of the aerosol mass, col+lected on the filter from an isokinetic sampler.

Wind speeds for use in characterizing sampling effectiveness of an inlet are suggested by the Environmental Protection Agency, Part 53, Subpart D to be: 0.56 m/s (2 km/h), 2.22 m/s (8 km/h), and 6.67 m/s (24 km/h); however, an additional speed was added to this test protocol, namely, 1.11 m/s. Ten μm AD particles is the reference size for most aerosol inlet studies.

The following experiments were conducted to fulfill the objectives based on the test procedures:

3.2.3.1. ***Testing the Battelle Inlet and the AWI-780***

1. Only the top chamber of the Battelle inlet and the AWI were tested to verify penetration through the system.
2. The effect of an internal cone, attached to the inside of the AWI roof was determined by testing the inlet with and without the internal cone.
3. The effect of the internal volume of the AWI's top chamber was determined by testing two different volumes.
4. Once the cutpoint of the current AWI was determined, studies to increase the cutpoint of the AWI were performed by changing a impactor jet diameter according to Equation (8).
5. The effect of the window area in a fractionator of the AWI was determined by testing four different window areas.
6. Several screen configurations were tested to determine the best screen configuration in terms of particle losses.
7. The effect of wind speed was verified because penetration of an acceptable inlet should not be greatly affected by different wind speeds.

8. A rain roof was fabricated for the Battelle inlet and the effect of the roof on the Battelle inlet was determined.

3.2.3.2. ***Testing the MIT Trigger Inlet and the AWI-90***

1. The effect of the intake gap was determined by testing three different gaps.
2. Several screen configurations were tested to determine the best screen configuration in terms of particle losses.
3. Studies to increase the cutpoint of the AWI were performed by changing a impactor jet diameter according to Equation (8).
4. The effect of wind speed was verified.
5. The effect of the internal volume of the AWI was verified by testing three different sizes of inlets.
6. The MIT-Fractionator system was tested.

Most data are in the form of penetration (%) as a function of either wind speed (km/h) or particle size (μm AD).

3.3. RESULTS AND DISCUSSION

3.3.1. Test Results – AWI-780

3.3.1.1. *Aerosol Penetration through the Top Chambers of the Battelle and AWI 780 L/min Units*

Table 4 shows the penetration of aerosol through the Battelle and the AWI-780 inlets. The AWI tested at this time was an initial version that had a cone fastened to the underside of the rain roof. For all three particle sizes – 5.2, 9.5, and 16.5 μm AD at the wind speed of 0.56 m/s (2 km/h), penetration of the Battelle inlet was very similar to that of the AWI.

Table 4. Comparison of Penetration of the Top Chamber of the Battelle Inlet with That of the AWI-780. Wind Speed: 2 km/h.

Particle Size	Battelle Inlet		AWI-780	
	Penetration, %	STD, %	Penetration, %	STD, %
4.9~5.4 μm AD	93.2	0.7	91.7	3.3
9.3~9.7 μm AD	83.5	2.0	81.0	2.4
16.5 μm AD	48.2	0.9	48.4	0.6

3.3.1.2. *Effect of an Internal Cone Attached to the Inside of the AWI-780 Roof*

Tests were conducted with and without the internal cone on the inside of the AWI roof. There was significant enhancement in the performance of the AWI without the cone, in terms of penetration (Figure 23). The concept of the internal cone was to make the flow stream downward, that way more particles will penetrate through the system. However, the result was vice versa due to the recirculation inside the top chamber. After these tests, the internal cone was removed for all further experiments. Figure 23 shows the penetration differences between the Battelle inlet and the AWI, with and without the internal cone.

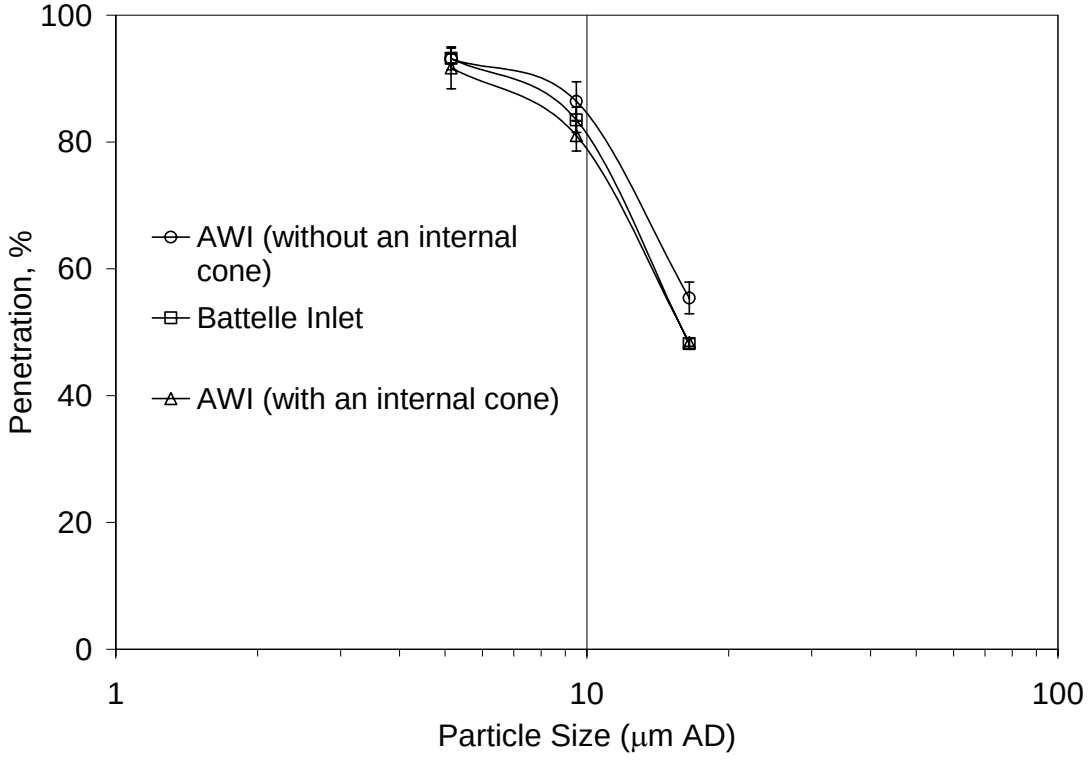

Figure 23. Penetration through the Top Chambers (without the Fractionator) of the Battelle and AWI-780 as a Function of Particle Size. Wind Speed: 8 km/h.

3.3.1.3. *Effect of the Internal Volume of the AWI-780 Top Chamber*

The internal volume of the basic AWI top chamber tested is 3435 cm³. A larger AWI's top chamber, with features identical to the basic AWI was fabricated, which had an internal volume of 11,558 cm³. Two different volumes of the AWI's top chambers were tested with about 10 μm AD particles, which is the reference size for this aerosol inlet study and compared (Table 5). There is a significant enhancement from use of a larger top chamber in terms of penetration. However, the size of an upgraded inlet should not be greatly exceeding that of the Battelle inlet. Internal volume of the Battelle inlet is 900 cm³. Therefore, a larger top chamber for the AWI may not be acceptable even though it allows more particles to penetrate.

Table 5. Effect of the AWI-780 Internal Volume of the Top Chamber.
Particle Size: 10.2 μm AD; Wind Speed: 8 km/h.

	AWI (I V: 3435 cm³)*	AWI (I V: 11,558 cm³)*
Penetration	81.4%	90.6%
STD	0.8%	2.1%

*I V: Internal Volume

3.3.1.4. *Effect of Different Vent Areas in an Internal Fractionator for the AWI-780*

The whole assembly, including the bottom chamber and internal fractionator along with the top chamber, was tested for both the Battelle inlet and the AWI-780. The optimum vent area in an internal fractionator for the highest penetration needs to be specified. The vent area of the Battelle inlet is 45.2 cm². The current AWI features a vent area of 207 cm² in the fractionator. Additionally, four different vent areas (145 cm², 290 cm², 436 cm², and 581 cm²) were available for experiments and Figure 24 examples two

vent areas in the fractionator. The AWI, with four different vent areas in the fractionator, was tested and Figure 25 shows the results. Among the four areas, the vent area of 145 cm² and 290 cm² had relatively higher penetrations than that of larger vent areas such as 436 cm² and 581 cm². These data suggest the impactor efficiency is better with larger vent area; however, the effect is not substantial – there is only about 10% difference in penetration over almost a four-fold change in vent area. Additionally, two vent areas of 207 cm² and 290 cm² were also compared (Table 6). The vent area of 207 cm² was chosen for the vent area because it resulted in the highest penetration through the fractionator.

Figure 24. Internal Fractionators – L) 581 cm², R) 290 cm².

Table 6. Comparison of Two Vent (Window) Areas for the AWI-780.
Particle Size: 10.2 μm AD; Wind Speed: 8 km/h.

	Area: 290 cm²	Area: 207 cm²
Penetration	48.5%	53.2%
STD	1.5%	2.4%

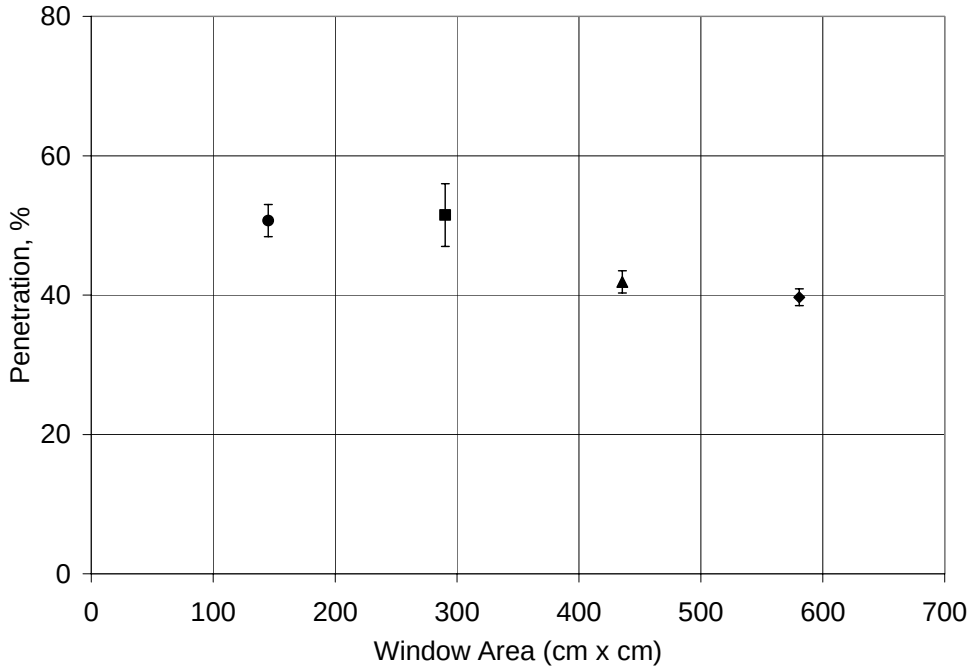

Figure 25. Effect of Vent Area in the Fractionator for the AWI-780.
Particle Size: 10.2 μm AD; Wind Speed: 8 km/h.

3.3.1.5. *Effect of Several Screen Configurations on the Battelle Inlet and the AWI-780*

The best screen should be determined so that it effectively blocks insects, yet allows particles to penetrate it in the size range of interest (1 to 10 μm aerodynamic diameter). With previous screens there were significant particle losses on the screens, so more research into screen efficiency needs to be done.

The Battelle inlet was being tested with a flat screen on top of the top chamber (Figure 26), but there were considerable particle losses due to the flat screen in the location. Therefore, an experiment on the Battelle inlet with a flat screen was conducted. An 8-mesh (8 holes per 2.54 cm (1 inch)) screen was used throughout this study and the wire thickness was 0.38 mm (0.015 inch). The flat screen caused around 40 % particle loss for 10.7 μm AD at 2.2 m/s, compared to the Battelle inlet without a screen (Figure 26). One can easily tell that the screen just filled the role of a kind of an impactor. This

was absolutely not an acceptable configuration. However, when the same flat screen was placed in the bottom chamber of the Battelle inlet, the result was quite vice versa. As shown in Table 7, only 8.9% particle loss was caused by the screen in the bottom chamber of the Battelle inlet.

Several different screen configurations – flat, conical, round cylindrical, and folded round cylindrical were fabricated and tested along with the AWI. Two screen configurations – flat and conical were used inside the top chamber and two screen configurations – round cylindrical and folded cylindrical were used for the internal fractionator. Finally, two screen configurations – conical and flat were used in the bottom chamber of the AWI.

In the top chamber of the AWI, a flat screen (Figure 27) and a conical screen (Figure 28) were tested for 11.2 μm AD at 2.2 m/s. While the penetration of the AWI without a screen was 36.2%, the penetrations for the flat and conical screens were 29.5% and 29.4%, respectively. In terms of particle loss, there was almost no difference between the two configurations. However, around 19% particle loss due to a bug screen is relatively high.

Three different screens were tested for the internal fractionator. A round cylindrical screen (Figure 29), with a diameter of 15.24 cm (6 inches) was placed inside the cup and a circumference screen (Figure 30) was placed outside of the cup, blocking all of the vent (window) area. Finally, a folded round cylindrical screen (Figure 31), with an inner diameter of 15.24 cm (6 inches) and an outer diameter of 20.32 cm (8 inches) was placed inside the cup. The AWI with each of the three screens was tested for 11.7

μm AD. Table 8 shows that there was still a significant amount of particle losses in all three cases.

Two different diameters (12.7 cm and 20.3 cm) of flat screens were placed at the bottom chamber (Figures 32 and 33, respectively) and a conical screen configuration (Figure 34) at the bottom chamber was also tested. Table 9 displays the data and the loss, due to a flat screen (diameter of 20.3 cm), was less than 5%, so the flat screen in this location could be the best option in terms of particle losses.

A flat screen configuration (diameter of 20.3 cm) in the bottom and the top chamber of the AWI was tested for different particle sizes – 6.4 μm, 11.2 μm, and 15.1 μm AD. As shown in Figure 35, the three data points with the flat screen in the bottom chamber are almost overlapped with those without the screen, but there are considerable particle losses due to the flat screen, placed in the top chamber – 14% losses for 6.4 μm AD and 18% losses for 11.2 μm AD, compared to penetrations without the flat screen.

Table 7. Effect of a Rain Roof and a Flat Screen on the Battelle Ilet. Wind Speed: 8 km/h.

	Battelle		Battelle		Battelle	
	No Screen		Flat Screen in Bottom Chamber		Flat Screen in Top Chamber	
	P. (%)	STD (%)	P. (%)	STD (%)	P. (%)	STD (%)
10.3 μm AD	38.3	2.2	34.9	0.6	26.3	0.2

Table 8. Effect of Several Screen Configurations on the AWI-780 Fractionator.
Particle Size: 11.7 µm AD; Wind Speed: 8 km/h.

	No Screen	Round Cylindrical (Inside Cup)	Round Cylindrical (Outside Cup)	Folded Cylindrical (Inside Cup)
Penetration	33.20%	28.20%	25.70%	21.40%
STD	0.50%	1.60%	0.80%	0.60%

Table 9. Effect of Several Screen Configurations on the AWI-780 Bottom Chamber.
Particle Size: 11.2 µm AD; Wind Speed: 8 km/h.

	No Screen	Flat 20.3 cm dia	Flat 12.7 cm dia	Conical
Penetration	35.90%	34.30%	32.10%	29%
STD	1.20%	0.30%	0.90%	0.90%

Flat Screen (15.2 cm diameter)
8 mesh
Wire thickness: 0.38 mm
Area of Screen: 182.6 cm²
Impactor jet ID: 4.9 cm

	No Screen	With screen
Penetration	39.5%	24.3%
STD	1.0%	0.9%

Particle Size: 10.7 µm AD
Wind Speed: 8 km/h

Figure 26. Performance of the Battelle Inlet with a Flat Screen across the Upper Chamber.

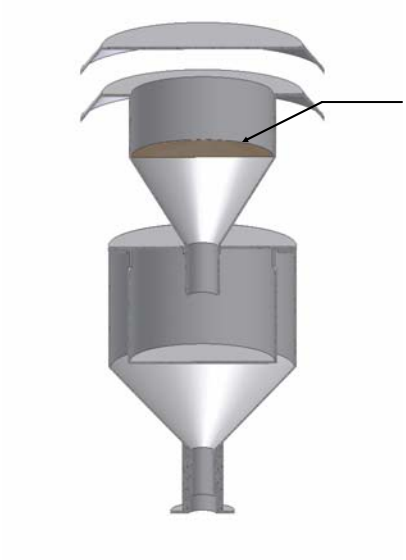

Flat Screen (20.3 cm diameter)
8 mesh
Wire thickness: 0.38 mm
Area of Screen: 304.5 cm²
Impactor jet ID: 4.9 cm

	No Screen		With Screen	
	P.	STD	P.	STD
6.4 µm AD	69.5%	2.1%	59.7%	3.9%
11.2 µm AD	36.2%	0.8%	29.5%	2.1%
15.1 µm AD	13.8%	0.2%	12.0%	0.4%

Wind Speed:8 Km/h

Figure 27. AWI-780 Inlet with a Flat Screen in the Lower Part of the Cylindrical Section of the Upper Chamber.

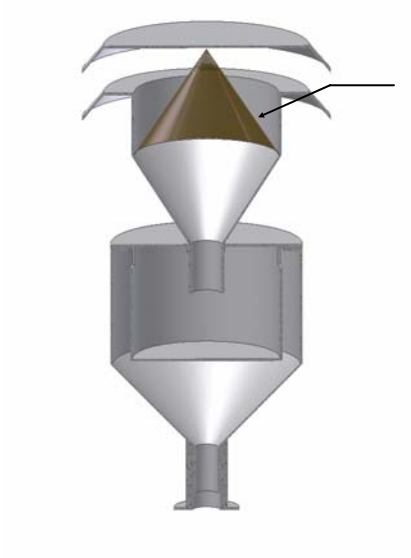

Cone type Screen
8 mesh
Wire thickness: 0.38 mm
Area of Screen : 425.2 cm²
Impactor jet ID: 4.9 cm

	No Screen	With screen
Penetration	36.2%	29.4%
STD	0.8%	0.3%

Particle Size: 11.2 µm AD
Wind Speed: 8 km/h

Figure 28. AWI-780 with a Conically-Shaped Screen in the Upper Chamber.

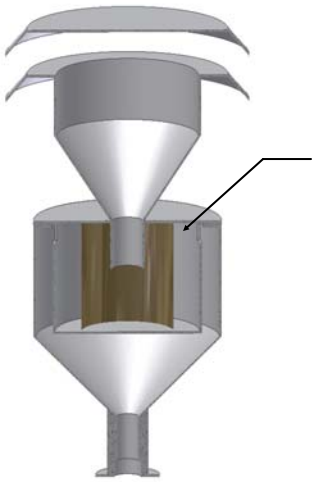

Round Cylindrical Screen
(15.2 cm diameter)
8 mesh
Wire thickness: 0.38 mm
Area of Screen: 631 cm²
Impactor jet ID: 4.9 cm

	No Screen	With screen
Penetration	33.2%	28.2%
STD	0.5%	1.6%

Particle Size: 11.7 µm AD
Wind Speed: 8 km/h

Figure 29. AWI-780 with a Cylindrical Shaped Screen Inside the Impactor Cup in the Lower Chamber.

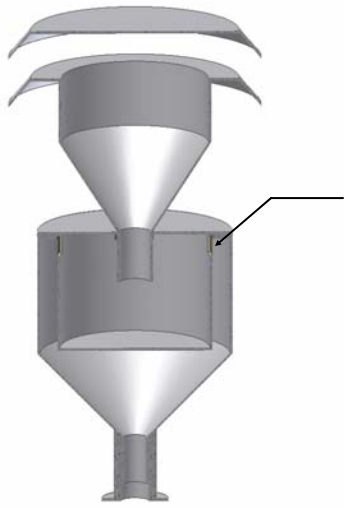

Circumference Screen
-Blocking all windows of Impaction Cup
8 mesh
Wire thickness: 0.38 mm
Area of Screen : 206.5 cm²
Impactor jet ID: 4.9 cm

	No Screen	With screen
Penetration	33.2%	25.7%
STD	0.5%	0.8%

Particle Size: 11.7 µm AD
Wind Speed: 8 km/h

Figure 30. AWI-780 with a Circumferential Screen on the Outside of the Impactor Cup. Screen Covers Windows in the Impactor Cup.

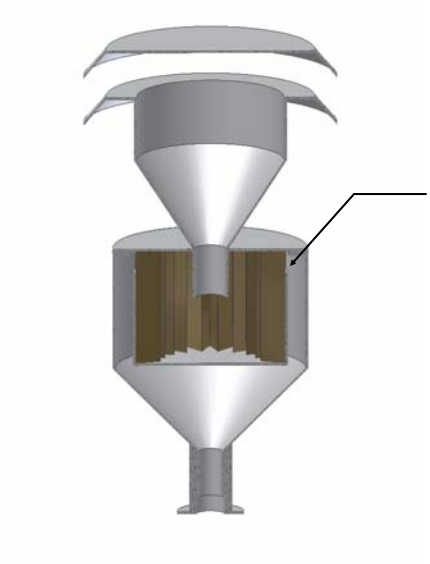

Pleated Cylindrical Screen
– Inner D: 15.24 cm; Outer D: 20.32 cm
8 mesh
Wire thickness: 0.38 mm
Area of Screen : 1256.8 cm²
Impactor jet ID: 4.9 cm

	No Screen	With screen
Penetration	33.2%	21.4%
STD	0.5%	0.6%

Particle Size: 11.7 µm AD
Wind Speed: 8 km/h

Figure 31. AWI-780 Inlet with a Pleated Cylindrically-Shaped Screen Inside the Impactor Cup in the Lower Chamber.

	No Screen	With screen
Penetration	35.9%	32.1%
STD	1.2%	0.9%

Particle Size: 11.2 µm AD
Wind Speed: 8 km/h

Flat Screen (12.7 cm diameter)
8 mesh
Wire thickness: 0.38 mm
Area of Screen : 126.5 cm²
Impactor jet ID: 4.9 cm

Figure 32. AWI-780 Inlet with a 12.7 cm Diameter Flat Screen in the Lower Chamber.

	No Screen		With Screen	
	P.	STD	P.	STD
6.4 µm AD	69.5%	2.1%	67.5%	1.1%
11.2 µm AD	36.2%	0.8%	34.3%	0.3%
15.1 µm AD	13.8%	0.2%	12.3%	0.4%

Wind Speed : 8 Km/h

Flat Screen (20.3 cm diameter)
8 mesh
Wire thickness: 0.38 mm
Area of Screen : 304.5 cm²
Impactor jet ID: 4.9 cm

Figure 33. AWI-780 with a 20.3 cm Diameter Flat Screen in the Lower Chamber.

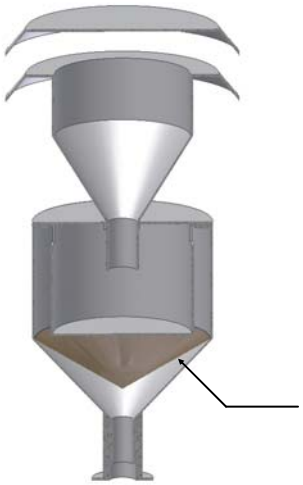

	No Screen	With screen
Penetration	35.9%	29%
STD	1.2%	0.9%

Particle Size: 11.2 µm AD
Wind Speed: 8 km/h

Cone type Screen
8 mesh
Wire thickness: 0.38 mm
Area of Screen : 608.1 cm²
Impactor jet ID: 4.9 cm

Figure 34. AWI-780 Inlet with a Conically-Shaped Screen in the Lower Chamber.

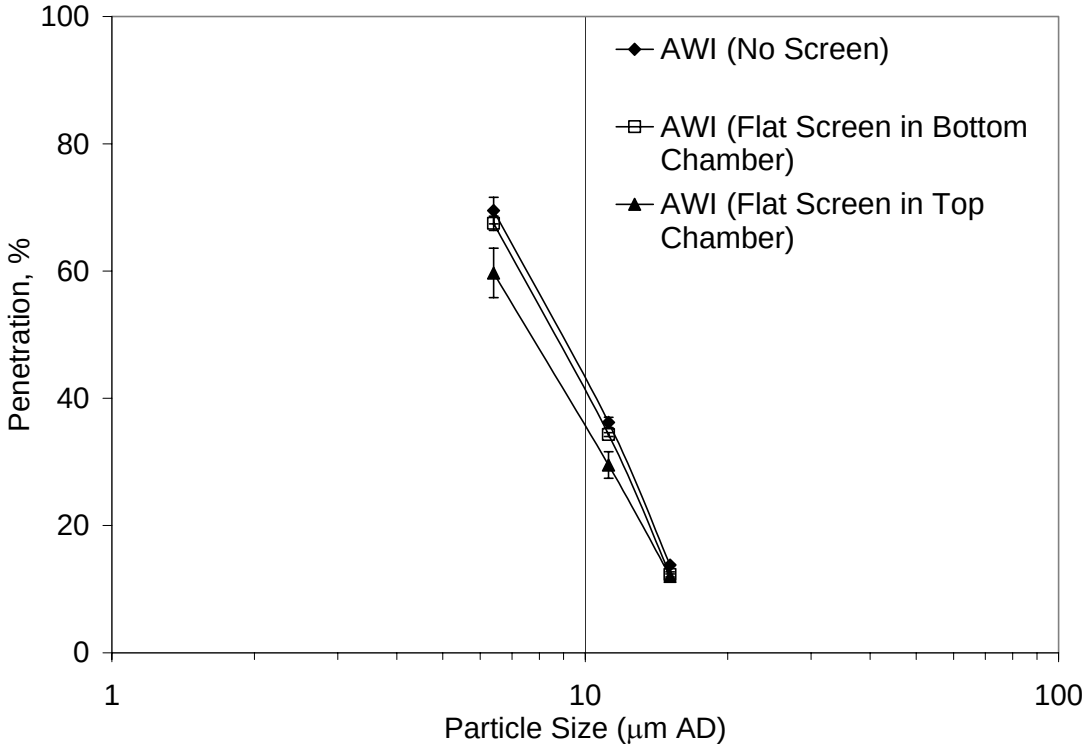

Figure 35. Penetration for the AWI-780 as a Function of Particle Size. Wind Speed: 8 km/h.

3.3.1.6. *Effect of the Impactor Jet Diameter for the AWI-780*

As shown in Figure 35, the cutpoint of the current AWI-780 (Jet ID: 4.93 cm) was about 9 μm AD. Therefore, there was an effort to increase a cutpoint to around 10 μm AD. According to Equation (8), an impactor jet diameter of 5.26 cm (2.07 inches) should have been used to obtain 10 μm AD cutpoint, but a jet diameter of 5.51 cm (2.17 inches) was considered because there will be particle losses due to a bug screen. As shown in Figure 36, the cutpoint of an AWI with a jet diameter of 5.51 cm is about 11 μm AD. During these tests, a bug screen was not installed in the AWI-780.

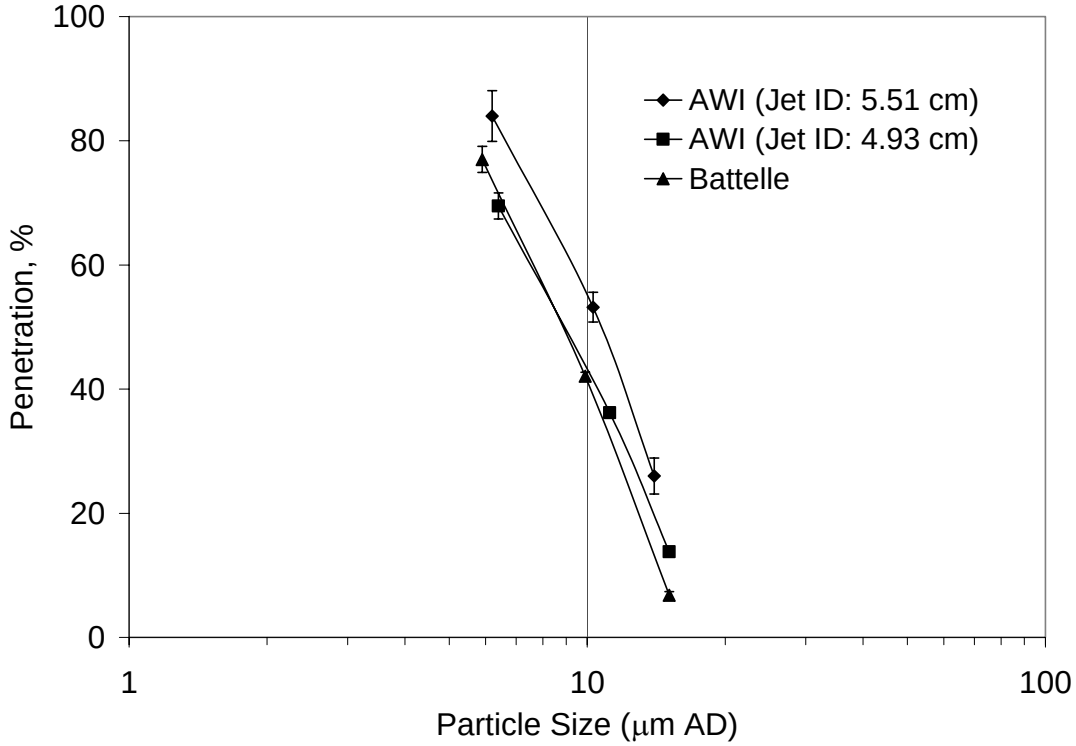

Figure 36. Penetration for the AWI-780 as a Function of Particle Size.
Wind Speed: 8 km/h.

3.3.1.7. *Effect of Wind Speed for the Battelle Inlet and the AWI-780*

The interest range of wind tunnel test speeds is from 2 to 24 km/h. An upgraded inlet should not be widely affected by wind speeds. As shown in Figure 37, there was 13% penetration difference between 2 and 24 km/h for the Battelle inlet. However, there was only 3% penetration difference between 2 and 24 km/h for the AWI-780 with jet diameters of 4.93 and 5.51 cm.

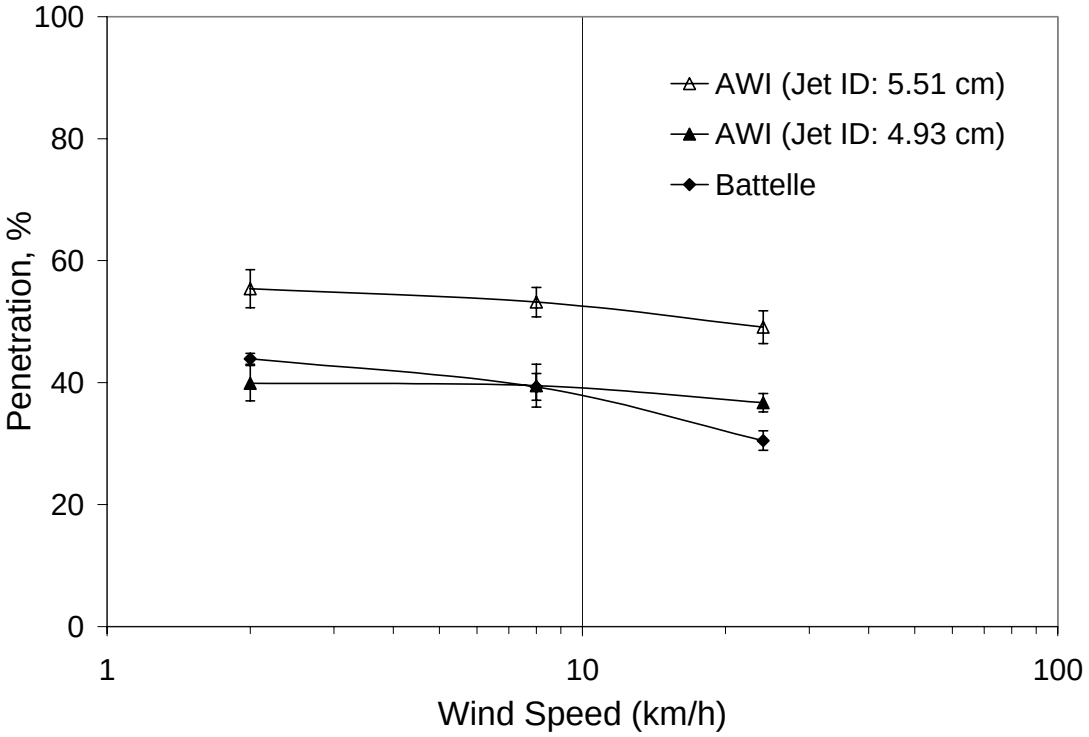

Figure 37. Penetration for the Battelle and the AWI-780 as a Function of Wind Speed. Particle Size: 10.3 μm AD.

3.3.1.8. *Effect of a Rain Roof on the Battelle Inlet*

A rain roof (Length: 30.5 mm) was installed on the top cover of the Battelle inlet and the inlet was tested with 10.3 μm AD at the wind speed of 8 km/h. Adding a rain roof to the Battelle inlet did not substantially change the penetration of the Battelle inlet – it was 38.3% without a rain roof and 36.1% with a rain roof. As a next step, the Battelle with the rain roof was tested for different wind speeds- 2 and 24 km/h to verify its wind sensitivity (Figure 38). The Battelle inlet with a rain roof deems to be a little more wind sensitive than that without a rain roof.

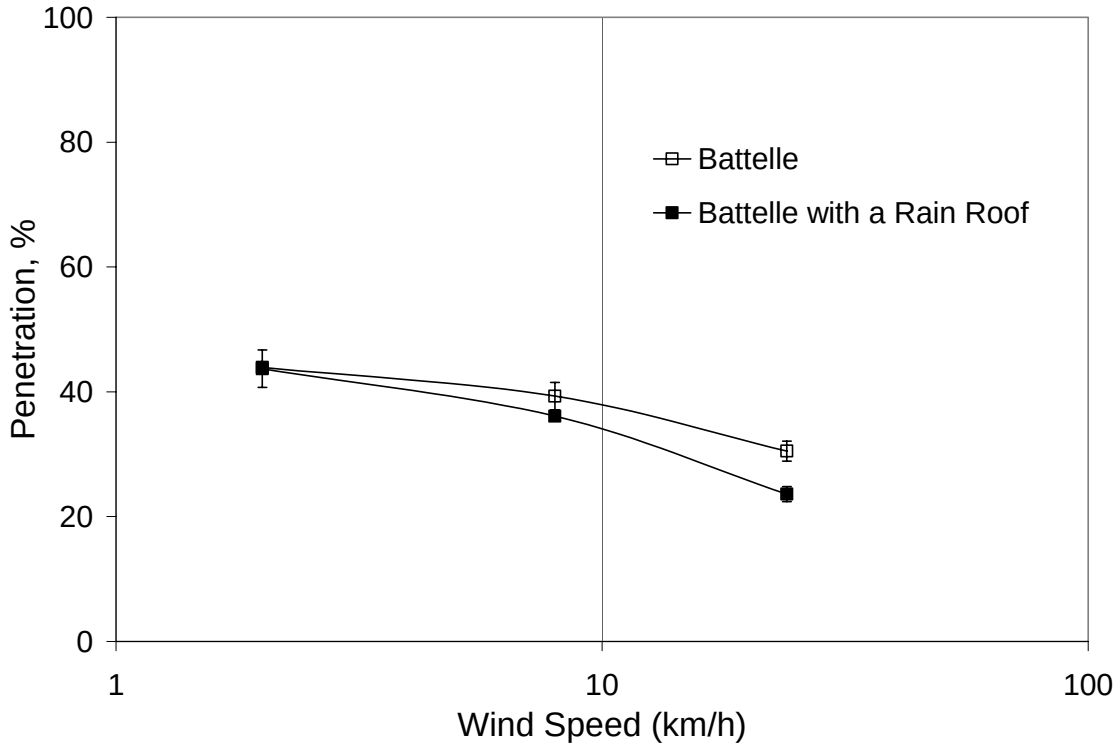

Figure 38. Penetration for the Battelle inlet with and without a Rain Roof as a Function of Wind Speed. Particle Size: 10.3 μm AD.

3.3.2. Test Results - AWI -90

3.3.2.1. *Effect of Intake Gap*

The AWI-90 with an intake gap of 4.1 mm (0.16 inch) was tested for three different particle sizes at 8 km/h. The height of 4.1 mm was tested to make the velocity at the flow entrance the same as that of the AWI-780. However, its cutpoint was slightly smaller than 10 μm AD (Figure 39). A cutpoint of the AWI-90 should be around 13 μm AD.

The intake gap was almost doubled (4.1 mm → 7.4 mm) and also tripled (4.1 mm → 10.7 mm). As shown in Tables 10a and 10b, there was a significant improvement in

terms of penetration when the height was doubled and test results were almost identical for 10.4 μm AD at 8 km/h between intake gaps of 7.4 and 10.7 mm.

Table 10a. Effect of Intake Gap of the AWI-90.
Particle Size: 10.6 μm AD; Wind Speed: 8 km/h.

	Intake Gap: 4.1 mm	Intake Gap: 7.4 mm	N/A
	AWI-90	AWI-90	MIT
Penetration, %	38.9	51.5	62.35
STD, %	1.2	0.6	0.4

Table 10b. Effect of Intake Gap of the AWI-90.
Particle Size: 10.4 μm AD; Wind Speed: 8 km/h.

	Intake Gap: 7.4 mm	Intake Gap: 10.7 mm	N/A
	AWI-90	AWI-90	MIT
Penetration, %	53.7	52.4	63.9
STD, %	2.9	1.1	1.9

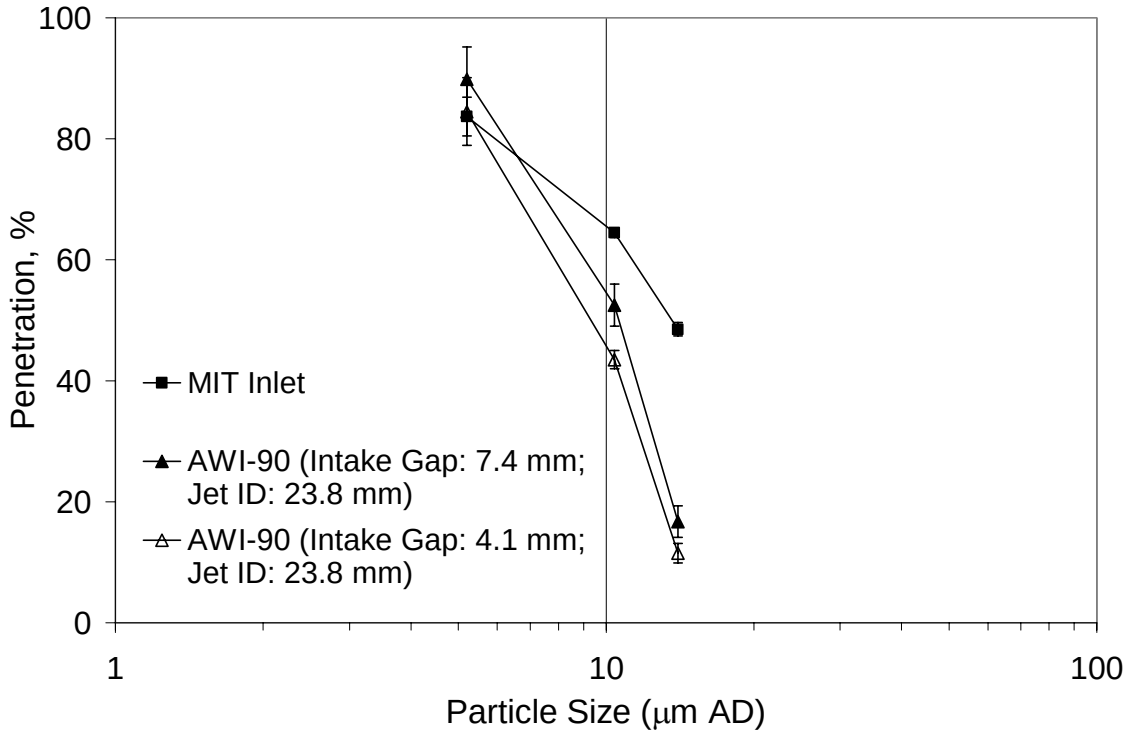

Figure 39. Penetration for the MIT and the AWI-90 as a Function of Particle Size for Different Intake Gaps. Wind Speed: 8 km/h.

3.3.2.2. *Effect of Screen on the AWI-90*

Three screen configurations were fabricated for the AWI-90. They are a flat screen inside the top chamber, a flat screen inside the bottom chamber, and a circumference screen outside the internal fractionator. An 8-mesh screen was used throughout this study and the thickness was 0.38 mm (0.015 inch). As shown in Table 11, a flat screen inside the bottom chamber was the best option in terms of particle losses – only 4% particle loss due to the screen. These results are consistent with that of the AWI-780.

Table 11. Effect of Several Screen Configurations for the AWI. Particle Size: 10.4 μm AD; Wind Speed: 8 km/h; Intake Gap: 7.4 mm; Impactor Jet Diameter: 23.8 mm.

	Flat in Top Chamber	Flat in Bottom Chamber	Round Cylindrical (Outside Cup)	No Screen	N/A
	AWI-90	AWI-90	AWI-90	AWI-90	MIT
Penetration, %	45.2	51.5	49.3	53.7	63.1
STD, %	0.2	1.3	1.6	2.9	2.2

3.3.2.3. *Effect of the Impactor Jet Diameter*

The cutpoint of the AWI-90 (Intake Gap: 7.4 mm and Impactor jet diameter: 23.8 mm) was between 10 and 11 μm AD. As previously mentioned the targeted cutpoint for the AWI is about 13 μm AD. Therefore, enlarged impactor jet diameters were tested and Equation (8) was used for calculations. For 15 μm AD and 20 μm AD cutpoints, impactor jet diameters of 30.2 and 36.6 mm were fabricated, respectively. The penetration became larger as the nozzle size was increased (Table 12). To verify more accurate cutpoint, tests with different sizes of particle such as 5 μm AD and 15 μm AD needs to be conducted.

Table 12. Effect of Impactor Jet Diameters. Intake Gap for the AWI-90: 7.4 mm; Particle Size: 10.4 μm AD; Wind Speed: 8 km/h.

	The AWI-90		
	Jet ID: 23.4 mm	Jet ID: 30.2 mm	Jet ID: 36.6 mm
Penetration, %	55.4	72.6	80
STD, %	2.1	1.5	0.1

3.3.2.4. *Effect of Wind Speed on Performance of the AWI-90*

As previously mentioned, the penetration of an inlet for ambient aerosol should not be greatly affected by the range of wind speeds form 2 to 24 km/h. The AWI-90 was tested for 2, 8, and 24 km/h and Figure 40 shows the results. For the AWI-90 with intake gaps of 4.1 and 7.4 mm, the penetrations for 10.4 μm AD at 8 km/h were 39 and 53%, respectively while those for the same particle size at 24 km/h were 15 and 22%, respectively. Penetration of the AWI-90 with the gap of 7.4 mm was reduced from 52.5% to 22% as wind speed was increased from 8 to 24 km/h. In contrast, the penetration difference between 8 and 24 km/h for the MIT inlet is about 18%. The above results indicate that the performance of the current AWI-90 is probably not acceptable.

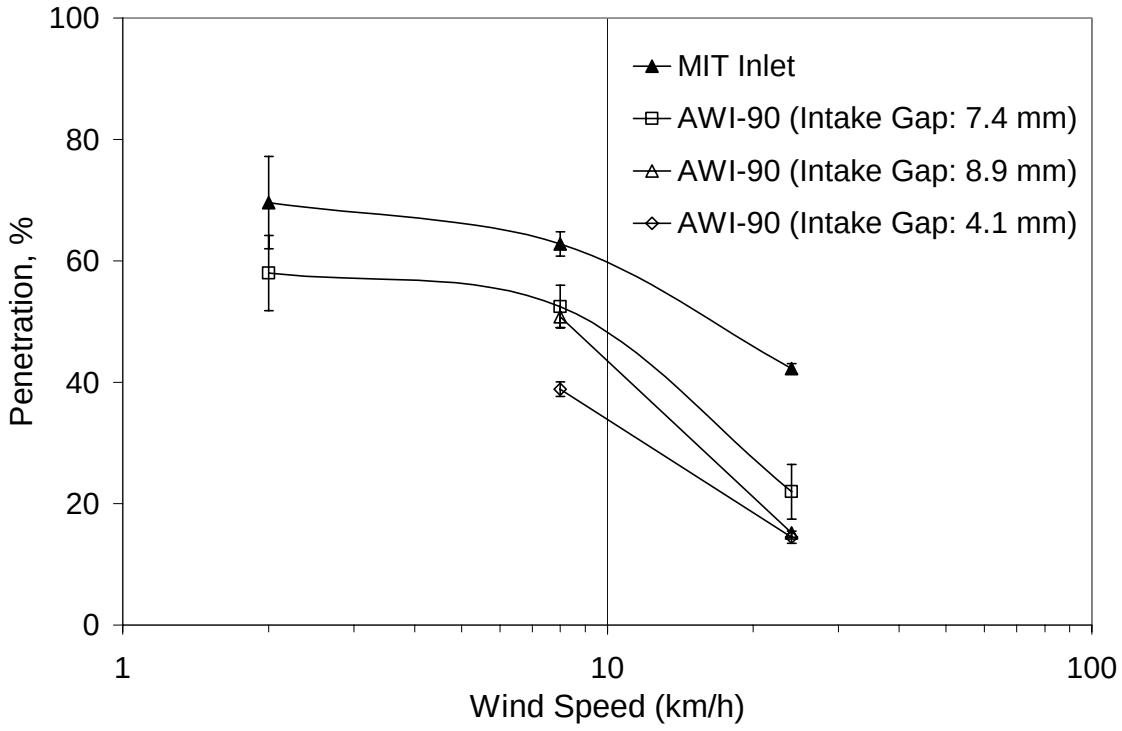

Figure 40. Penetration for the MIT and the AWI-90 without the Fractionator as a Function of Wind Speed for Different Intake Gaps. Particle Size: 10.4 μm AD.

3.3.2.5. *Effect of the Internal Volume of the Top Chamber*

The current AWI-90 which is one-third scaling of the AWI-780 is unacceptable because it is greatly affected by wind speeds, especially between 8 and 24 km/hr.

Different sizes of top chambers were tested to verify their performance as a function of wind speed. For these tests, the fractionator and impactor jet were removed. Three volumes – one third, two thirds, and one full scaling of the AWI-780 were tested at a flowrate of 0.0015 m^3/s (90 L/min). As shown in Figure 41, performance of the two thirds unit was much enhanced in terms of penetration, compared to the AWI-90, but there is still significant penetration difference between the wind speed of 8 and 24 km/h. Both the 2/3 and full scale AWI-780 bodies had penetration values >50% over the full range of wind speeds, which suggests that these bodies, if fitted with fractionators, could provide cutpoints of at least 10 μm AD.

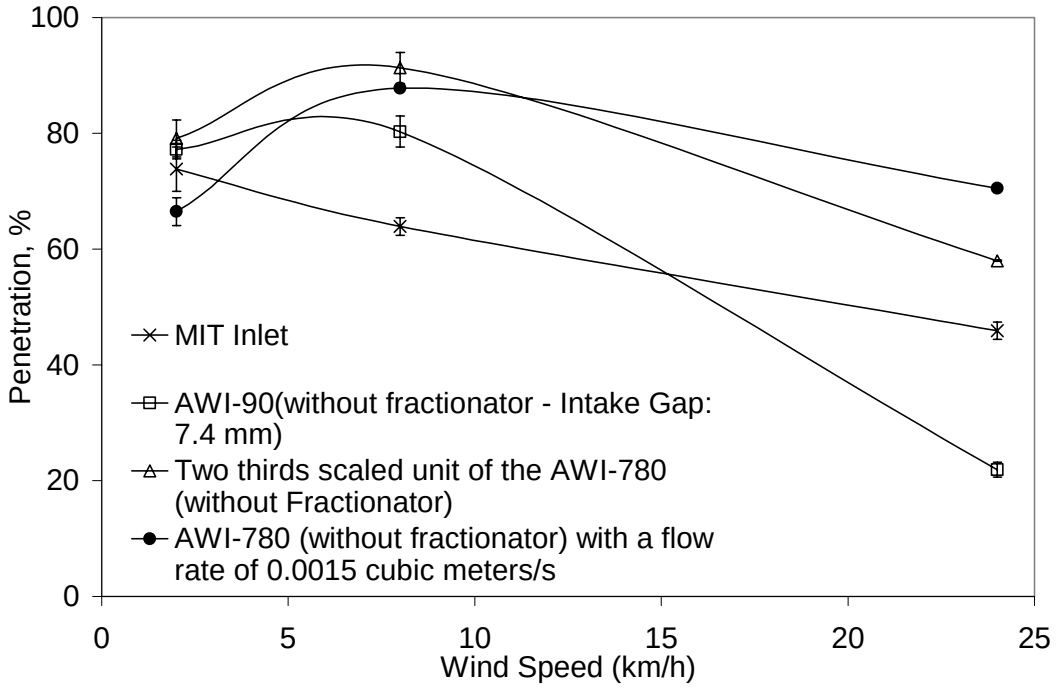

Figure 41. Penetration for the MIT, AWI-90, Two Thirds Scaled Unit of the AWI-780, and AWI-780 as a Function of Wind Speed. Particle Size: 10.4 μm AD.

3.3.2.6. *MIT-Fractionator System*

The MIT inlet shows less wind sensitivity than either the two thirds scaled unit of the AWI-780 or the AWI-90, so as approach to obtaining a means for preventing entry of debris through the MIT inlet, the fractionator of the AWI-90 was couples to the MIT inlet (Figure 42). The MIT-Fractionator system was tested at three wind conditions (Figure 43) and with three particle sizes (Figure 44). Adding the fractionator to the MIT inlet trends to flatten the curve of penetration as a function of wind speed (Figure 43), and it reduces the penetration of large particles (15.8 μm AD) (Figure 44).

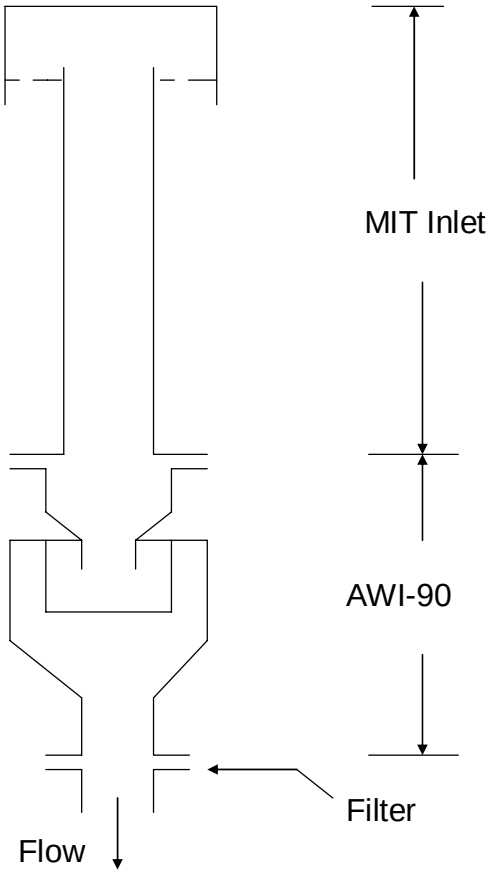

Figure 42. The MIT-Fractionator System (Impactor Jet ID: 30.2 mm).

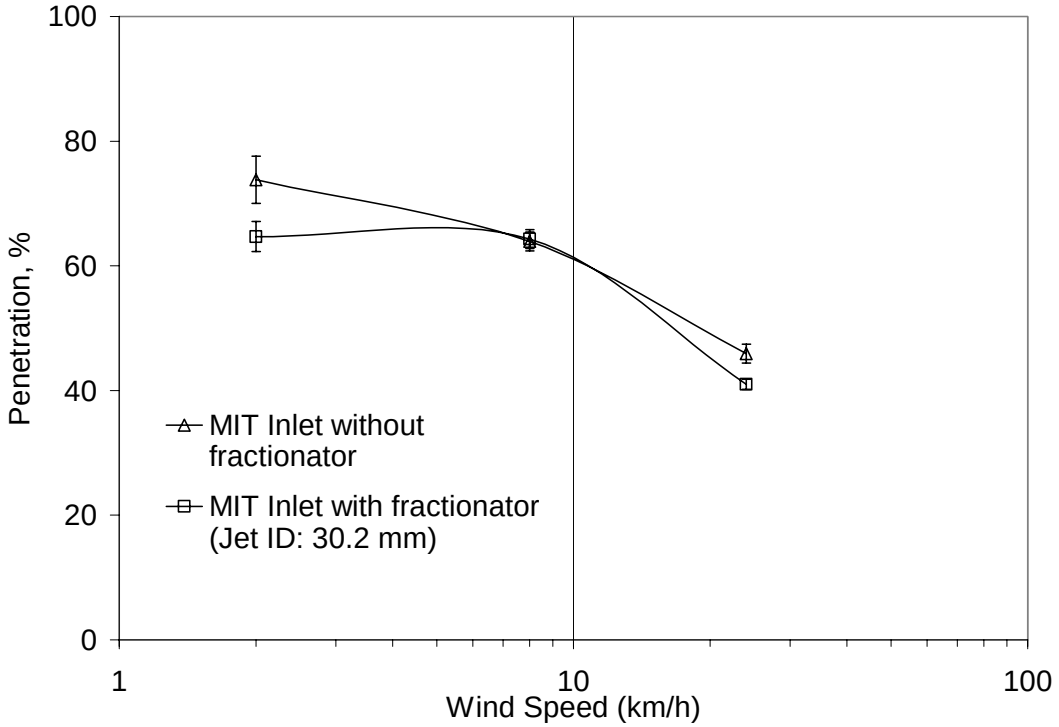

Figure 43. Penetration for the MIT inlet with and without Fractionator as a Function of Wind Speed. Particle Size: 10.4 μm AD.

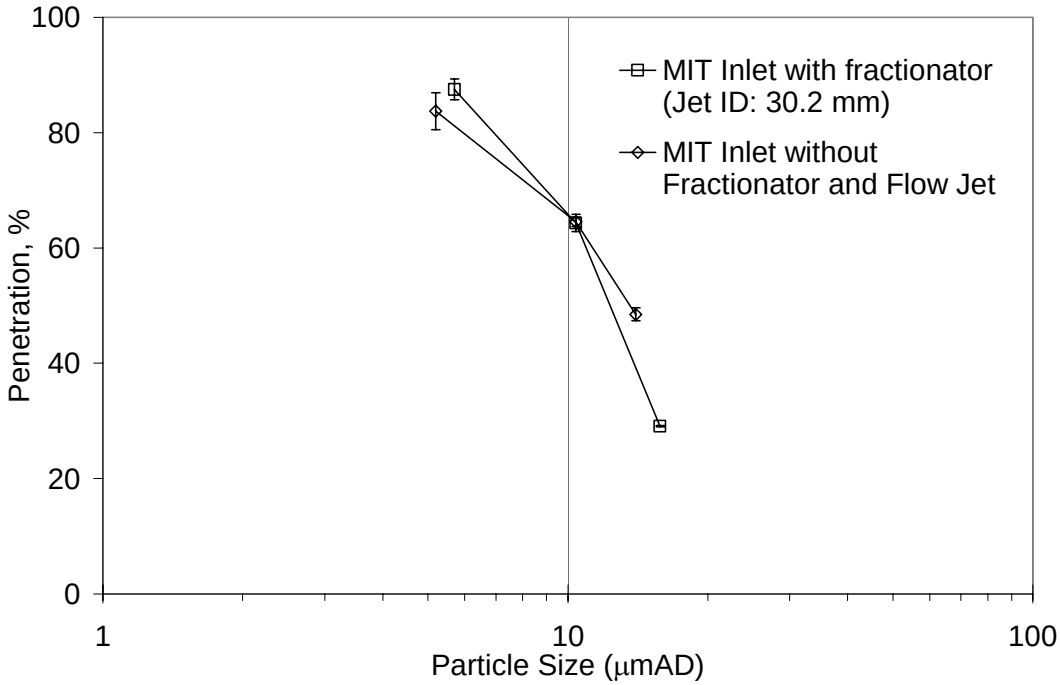

Figure 44. Penetration for the MIT inlet with and without Fractionator as a Function of Particle Size. Wind Speed: 8km/h.

3.4. QUALITY ASSURANCE

When measuring flowrates, rotameters (Dwyer Instruments, Michigan City, IN) were used. Before being used, the rotameters were calibrated by using a Roots meter (Model 5M 125 TC, Dresser Measurement, Houston, TX) and the pressure drop of the flow system was measured by Magnehelic Differential Pressure Gages (Dwyer Instruments, Michigan City, IN). After the pressure drop was determined, the flowrate was corrected for pressure and an equation for the correction followed:

$$Q_2 = Q_1 \times \sqrt{\frac{P_2}{P_1}} \tag{11}$$

where Q_1 is the observed flowmeter reading, Q_2 is the actual flow corrected for pressure, P_1 is the standard atmospheric pressure (101.3 kPa), and P_2 is the actual pressure, which is the standard atmospheric pressure minus the pressure inside of flowmeter.

Since particle sizing was a critical part of this study, there were several careful steps that had to be taken. Since the test aerosol was liquid, the flattening factor, which is the ratio of apparent drop diameter on a microscope slide to the true diameter of the spherical drop, had to be accounted for. The sodium fluorescein was added on a ratio of 10% of solute and for sodium fluorescein concentrations within the range of 0%-20%, the effect of the presence of this additive upon the flattening coefficient is negligible and is 1.32 for oleic acid (Olan-Figueroa et al., 1982). The microscope slides were made oil-phobic by immersion in a fluorocarbon surfactant (NYE BAR Type K 0.2%). At the beginning and end of each test, oleic acid aerosol droplets were collected on a coated microscope slide and analyzed with an optical microscope to verify the aerosol particle size. An optical microscope was calibrated by a micro stage scale before particle sizing.

An aerodynamic particle sizer (Model 3310, TSI, Inc., Shoreview, MN) was used to assure that the aerosol particle size remained constant. The aerodynamic diameter (AD) was calculated by:

$$D_a = D_p \times (\frac{\rho_p}{\rho_0})^{\frac{1}{2}} \qquad (12)$$

where, D_p is the physical diameter of the droplets, ρ_p is the density of the droplets, and ρ_0 is the standard particle density, 1000 kg/m³. Here, the density of the droplets, comprised of a mixture of 90% oleic acid and 10% sodium fluorescein was 933 kg/m³.

When a fluorometer (Turner Quantech Digital Filter Fluorometer - Model 450, Barnstead International, Dubuque, IA) was used for fluorescein analysis, the following steps were employed. Kesavan et al. studied factors that affect fluorescein analysis and confirmed or demonstrated the following: (1) the optimum excitation and emission wavelengths for fluorescein are 492 nm and 516 nm, respectively; (2) the fluorescein intensity from a fluorescein solution is strongly pH dependent, but for values of pH above 9 the intensity is both maximized and constant (Kesavan et al., 2001). By using the NB490 and SC515 filters and adding one drop of 1 N NaOH to each 5 mL sample of liquid, the above requirements were fulfilled.

CHAPTER IV

SUMMARY AND CONCLUSIONS

4.1. DEGREE OF MIXING DOWNSTREAM OF RECTANGULAR BENDS

The focus of this study is on evaluation of mixing square and rectangular ductwork with respect to generating conditions that are suitable for single point representative sampling as defined by ANSI N13.1. In previous studies that we have performed on using results with scale models to predict the mixing in prototype ducting, we generally set a limit of acceptability of about 10% for the *COV*s of velocity and tracer gas concentration even though the ANSI N13.1 criterion is 20%. This margin of error is intended to accommodate any subtle physical differences between model and prototype, and the additional errors that are inherent with field testing as compared with laboratory evaluations.

Tests with a straight square duct that was not preceded by a mixing element showed a COV for tracer gas of 143% at a distance of 19 hydraulic duct diameters downstream from the gas injection point. When a single 90° mitred bend is placed upstream of the straight duct, the *COV* for tracer gas is reduced to 24.3% at a distance of 9.5 duct diameters downstream (Top Inside release). But, when turning vanes are placed inside the 90° mitred bend, the tracer gas COV increases to 86% at the 9.5 duct diameter location (Top Outside release). If a U-shaped double mitred bend is used as a mixing element, its mixing effect was almost the same as the effect of a single 90° bend. However, the degree of mixing downstream of an S-type double square bend is

significantly enhanced compared with other configurations. Even at 6 duct diameters downstream of the S-type double square bend, the *COV*s of velocity and SF_6 concentration are 10.6% and 8.3% (Top Inside release), respectively, which is acceptable for single-point representative air sampling.

Comparisons between the *COV*s for square and circular ducts with a curvature ratio (radius of the bend to the tube radius) of 2.0 show similar results, particularly for distances greater than about 7 duct diameters from the exit plane of a 90° bend. However, at distance of 3 hydraulic diameters downstream from the bend the gas *COV* for the circular duct is 69% (Center release), while that for the square duct is 83% (Center release).

Tests conducted with a rectangular duct (3:1 aspect ratio) showed poorer mixing than the square duct. At a distance of 9 hydraulic diameters from the exit plane of a 90° bend (turning axis was the short dimension of the aspect ratio), the *COV*s of velocity and tracer gas were 29% and 62% (Bottom Inside release), respectively for the rectangular duct while the velocity and tracer gas values for the square duct were 6.4% and 28% (Top Inside release), respectively.

Pressure loss across the mixing elements was tested. The pressure coefficient in a single 90° mitred bend without turning vanes was 4 times as large as that when turning vanes were used; however, the mixing is much poorer when vanes are used in the bend. The pressure loss in an S-type double bend is about 10 times as large as a single bend with turning vanes.

4.2. DESIGN OF AN INLET FOR AMBIENT AEROSOL

This study has been conducted to design, develop, and test bioaerosol sampling inlets. The Battelle system has two inlets, one that samples at a flowrate of 0.013 m^3/s (780 L/min), which is operated only when the fluorescent trigger fed by aerosol inlet (flowrate of 90 L/min) detects an anomalous response.

The penetration of the 780 L/min Battelle inlet was slightly higher than that of the first version of the unit developed herein, the AWI-780. Because one of the objectives was that penetration of the upgraded inlet should be at least equal or higher than the original Battelle inlet, the original AWI-780 needed to be modified. The original AWI-780 featured an internal cone, attached to the inside of the AWI roof, which was then removed. After removing the cone, the penetration of the AWI-780 was higher than that of the Battelle inlet - 81% with the cone while 86% without the cone for around 9.5 µm AD particles at 2 km/h. Neither inlet had a fractionator for these tests. Different particle sizes such as 5 and 16.5 µm were tested and similar results were obtained.

Internal volume of the AWI-780 was 3435 cm^3 and a larger AWI top chamber, with features identical to the AWI-780, having an internal volume of 11,558 cm^3 was fabricated. Two different sizes of top chambers were tested with about 10 µm AD particles and there was a significant enhancement in penetration from use of a larger top chamber for the AWI. However, the size of an upgraded inlet should not be considerably greater than the original Battelle inlet. Therefore, a larger top chamber for the AWI may not be effective even though it shows higher penetration.

The optimum vent area in an internal fractionator, which causes the highest penetration, needed to be specified. Four different vent areas (145 cm^2, 290 cm^2, 436 cm^2,

and 581 cm²) were tested and the vent area of 145 cm² and 290 cm² had relatively higher penetrations than that of larger vent areas such as 436 cm² and 581 cm². Additionally, two vent areas of 207 cm² and 290 cm² were also compared and the vent area of 207 cm² was selected because it resulted in the highest penetration through the fractionator.

There are significant particle losses due to a bug screen and the best screen should be determined that effectively blocks insects yet allows particles to penetrate through it in the size range of interest (1 to 10 μm AD). Flat, conical, cylindrical, and folded cylindrical were fabricated and tested along with the AWI-780 and the Battelle inlet. Results showed that a flat screen in the bottom chamber was the best configuration for both the Battelle inlet and the AWI in terms of particle loss – less than 5% loss for particles with region of 10 - 11 μm AD at a wind speed of 8 km/h.

The AWI-780's impactor jet diameter was originally 4.9 cm and the cutpoint with the jet diameter was less than 10 μm AD. Because the target cutpoint for the AWI-780 is 10 μm AD, there was an effort to increase its cutpoint to 10 μm AD. According to Equation (8), a impactor jet diameter of 5.26 cm (2.07 inches) should have been used to obtain 10 μm AD cutpoint, but a impactor jet diameter of 5.51 cm was tested to have around 11 μm AD cutpoint because a flat screen in the bottom chamber causes around 5% particle losses. Therefore, the AWI-780 with a jet diameter of 5.51 cm (2.17 inches) was tested and provided a cutpoint of about 11 μm AD.

The penetration of the enhanced inlet should not be a function of wind speed. The interest range of wind speed is from 2 to 24 km/h and there was only 3% penetration difference between 2 and 24 km/h for the AWI-780 with a jet diameter of either 4.93 or 5.51 cm.

An optimum intake gap for the AWI-90 had to be determined and three different heights such as 4.1, 7.4, and 10.7 mm were tested. Among those, the height of 7.4 mm was the best choice in terms of penetration.

A flat screen inside the top chamber, a flat screen inside the bottom chamber, and a circumference screen outside the internal fractionator were tested and a flat screen inside the bottom chamber was the best option in terms of particle losses. These results are consistent with that of the AWI-780.

A cutpoint of the AWI-90 (Intake Gap: 7.4 mm and Impactor jet diameter: 23.8 mm) was between 10 and 11 μm AD and the targeted cutpoint for the AWI is at least or equal to 13 μm AD. Impactor jet diameters of 30 and 36.6 mm were tested for 15 and 20 μm AD cutpoint, respectively. The cutpoint became larger as the nozzle size was increased. The AWI-90 with the jet diameters of 30 and 36.6 mm needs to be tested for 5 and 15 μm AD particles to verify its cutpoint in the future.

The AWI-90, at one-third scaling of the AWI-780, was widely affected by different wind speeds such as 8 and 24 km/h. Three volumes – one-third, two-thirds, and one full scaling of the AWI-780 were tested. At this time, the fractionator and an impactor jet were removed. Performance of the two-thirds scaled unit was much enhanced in terms of penetration, compared to the AWI-90, but there is still significant penetration difference between the wind speed of 8 and 24 km/h. The MIT inlet shows less wind sensitivity than both the AWI-90 and the two-third scaled inlets. Therefore, the fractionator was added to the MIT (MIT-Fractionator system) and when the system was tested for three wind conditions and three particle sizes, presenting the fractionator to the MIT inlet does not affect the performance of the MIT in terms of penetration.

REFERENCES

American National Standards Institute (1969). *Guide to Sampling Airborne Radioactive Material in Nuclear Facilities*. ANSI Standard N13.1, ANSI, New York, NY.

Anand, M., McFarland, A.R., and Rajagopal, K.R. (2003). Gas Mixing for Achieving Suitable Conditions for Single Point Aerosol Sampling in a Straight Tube: Experimental and Numerical Results. *Health Physics* 84: 82-91.

ASHRAE (1989). *Fundamentals. 1989 ASHRAE Handbook*. American Society of Heating, Refrigerating and Air Conditioning Engineers, Inc. Atlanta, GA.

Ballinger, M.Y., Barnett, J.M., Glissmeyer, J.A., and Edwards, D.L. (2004). Evaluation of Sampling Locations for Two Radionuclide Air-Sampling Systems Based on the Requirements of ANSI/HPS N 13.1-1999. *Health Physics* 86:406-415.

Berglund, R.N., and Liu, B.Y.H. (1973). Generation of Monodisperse Aerosol Standards. *Environ. Sci. Tech*. 7:147-153.

Chandra, S., and McFarland, A.R. (1997). Shrouded Probe Performance: Variable Flow Operation and Effect of Free-Stream Turbulence, *Aerosol Sci. Technol.* 26:111-126

Fan, B.J., Wong, F.S., Ortiz, C.A., Anand, N.K., and McFarland, A.R. (1993) Aerosol Particle Losses in Sampling Systems. 22nd DOE/NRC Air Cleaning Conference. NUREG/CP-0130, CONF9020823. Harvard School of Public Health, Boston, MA.

Fox, R.W., and McDonald, A.T. (2001). *Introduction to Fluid Mechanics*, Fifth Edition. John Wiley & Sons, Inc. New York.

Gupta, R. (1999). Turbulent Mixing and Deposition Studies for Single Point Aerosol Sampling. Ph.D. Dissertation. Department of Mechanical Engineering, Texas A&M University, College Station.

Hampl, V., Niemela, R., Shulman, S., and Bartley, D.L. (1986). Use of Tracer Gas Technique for Industrial Exhaust Hood Efficiency Evaluation – Where to Sample? *Am. Ind. Hyg. Assoc. J.* 47:281-287.

Health Physics Society (1999). Sampling and Monitoring Releases of Airborne Radioactive Substances from the Stacks and Ducts of Nuclear Facilities. ANSI/HPS N13.1-1999, McLean, VA.

Hinds, W.C. (1999). *Aerosol Technology*, John Wiley & Sons, New York.

Kesavan, J., Doherty, R.W., Wise, D.G., and McFarland, A.R. (2001). Factors That Affect Fluorescein Analysis, Edgewood Chemical Biological Center, U.S. Army Soldier and Biological Chemical Command, Final Report ECBC-TR-208, Edgewood, MD.

McFarland, A.R., Anand, N.K., Ortiz, C.A., Gupta, R., Chandra, S., and McManigle, A.P. (1999a). A Generic Mixing System for Achieving Conditions Suitable for Single Point Representative Effluent Air Sampling. *Health Physics* 76: 17-26

McFarland, A.R., Gupta, R., and Anand, N.K. (1999b). Suitability of Air Sampling Locations Downstream of Bends and Static Mixing Elements. *Health Physics* 77: 703-712.

McFarland, A.R., Ortiz, C.A., Moore, M.E., DeOtte, R.E., and Somasundaram. S. (1989). A Shrouded Aerosol Sampling Probe. *Environ. Sci. Tech*. 23: 1487-1492.

McFarland, A.R., and Rodgers, J.C. (1993). Single Point Representative Sampling with

Shrouded Probes. Report LA-12612-MS. Los Alamos National Laboratory, Los Alamos, NM.

Olan-Figueroa, E., McFarland, A.R., and Ortiz, C.A. (1982). Flattening Coefficient for DOP and Oleic Acid Droplets Deposited on Treated Slides, *Am. Ind. Hyg. Assoc. J.* 43:395-399.

Rodgers, J.C., Fairchild, C.I., Wood, G.O., Ortiz, C.A., Muyshondt, A., and McFarland, A.R. (1996). Single Point Aerosol Sampling: Evaluation of Mixing and Probe Performance in a Nuclear Stack. *Health Physics* 70:25-35.

U.S. Environmental Protection Agency. (1999). Procedures for Testing Performance Characteristics of Methods for PM_{10}. *Code of Federal Regulations*, Protection of Environment – Part 53, Subpart D. U.S. Government Printing Office, Washington, DC.

U.S. Environmental Protection Agency. (2000a). Method 5 – Determination of Particulate Matter Emissions from Stationary Sources. *Federal Register* 65: No. 201: 61831 - 61854. October 17, 2000.

U.S. Environmental Protection Agency. (2000b). Method 17 – Determination of Particulate Matter Emissions from Stationary Sources. *Federal Register* 65: No. 201: 62003-62006. October 17, 2000.

U.S. Environmental Protection Agency. (2000c). Method 1-Sample and Velocity Traverses for Stationary Sources. *Federal Register* 65: No. 201: 61779 – 61787. October 17, 2000.

U.S. Environmental Protection Agency. (2003d). National Emission Standards for Emissions of Radionuclides other than Radon from Federal Facilties. *Code of*

Federal Regulations, 40 CFR 61, Subpart H. U.S. Government Printing Office, Washington, DC.

U.S. Environmental Protection Agency. (2003e). National Emission Standards for Emissions of Radionuclides from Federal Facilities other than Nuclear Regulatory Commission Licensees that are not Covered by Subpart H. *Code of Federal Regulations*, 40 CFR 61, Subpart I. U.S. Government Printing Office, Washington, DC.

Other Sources Consulted

Chandra, S. (1992). Experimental Investigation into Operational Characteristic of a Shrouded Probe for Aerosol Sampling. M.S. Thesis, Department of Mechanical Engineering, Texas A&M University, College Station, TX.

McFarland, A.R., Gong, H., Muyshondt, A., Wente, W.B., and Anand, N.K. (1997), Aerosol Deposition in Bends with Turbulent Flow. *Environ. Sci. Tech*. 31:3371-3377.

Tolocka, M.P., Peters, T.M., Vanderpool, R.W., Chen, F., and Wiener, R.W. (2001). On the Modification of the Low Flow-Rate PM10 Dichotomous Sampler Inlet. *Aerosol Sci. Tech.* 34:407-415.

VITA

Name:	**Youngjin Seo**
Date and Place of Birth:	February 2, 1977 Taegu, Korea
Permanent Address:	848-11 Manchon-3-dong, SusungGu, Taegu, Korea 706-023
Education:	B.S. in Aeronautical and Mechanical Engineering, Hankuk Aviation University, Koyang, Korea, 2002 M.S. in Mechanical Engineering, Texas A&M University, College Station, Texas, 2004